

Circumstellar C₂, CN, and CH⁺ in the optical spectra of post-AGB stars ^{★ ★★}

Eric J. Bakker^{1,2,3}, Ewine F. van Dishoeck⁴, L.B.F.M. Waters^{5,6}, and Ton Schoenmaker⁷

¹ University of Texas, Department of Astronomy, TX78712, USA

² Astronomical Institute, University of Utrecht, P.O. Box 80000, NL-3508 TA Utrecht, The Netherlands

³ SRON Laboratory for Space Research, Sorbonnelaan 2, NL-3584 CA Utrecht, The Netherlands

⁴ Sterrewacht Leiden, University of Leiden, P.O. Box 9513, NL-2300 RA Leiden, The Netherlands

⁵ Astronomical Institute, University of Amsterdam, Kruislaan 403, NL-1098 SJ Amsterdam, The Netherlands

⁶ SRON Laboratory for Space Research, P.O. Box 800, NL-9700 AV Groningen, The Netherlands

⁷ Kapteyn Sterrenwacht Roden, Mensingheweg 20, NL-9301 KA Roden, The Netherlands

Received 16 April 1996/ October 2 1996

Abstract. We present optical high-resolution spectra of a sample of sixteen post-AGB stars and IRC +10216. Of the post-AGB stars, ten show C₂ Phillips (A¹Π_u – X¹Σ_g⁺) and Swan (d³Π_g – a³Π_u) and CN Red System (A²Π – X²Σ⁺) absorption, one CH⁺ (A¹Π – X¹Σ⁺) emission, one CH⁺ absorption, and four without any molecules. We find typically $T_{\text{rot}} \sim 43 - 399, 155 - 202$, and $18 - 50$ K, $\log N \sim 14.90 - 15.57, 14.35$, and $15.03 - 16.47$ cm⁻² for C₂, CH⁺, and CN respectively, and $0.6 \leq N(\text{CN})/N(\text{C}_2) \leq 11.2$. We did not detect isotopic lines, which places a lower limit on the isotope ratio of ¹²C/¹³C > 20. The presence of C₂ and CN absorption is correlated with cold dust ($T_{\text{dust}} \leq 300$ K) and the presence of CH⁺ with hot dust ($T_{\text{dust}} \geq 300$ K). All objects with the unidentified 21 μm emission feature exhibit C₂ and CN absorption, but not all objects with C₂ and CN detections exhibit a 21 μm feature. The derived expansion velocity, ranging from 5 to 44 km s⁻¹, is the same as that derived from CO millimeter line emission. This unambiguously proves that these lines are of circumstellar origin and are formed in the AGB ejecta (circumstellar shell expelled during the preceding AGB phase). Furthermore there seems to be a relation between the C₂ molecular column density and the expansion velocity, which is attributed to the fact that a higher carbon abundance of the dust leads to a more efficient

acceleration of the AGB wind. Using simple assumptions for the location of the molecular lines and molecular abundances, mass-loss rates have been derived from the molecular absorption lines and are comparable to those obtained from CO emission lines and the infrared excess.

Key words: molecular processes — circumstellar matter — stars: AGB and post-AGB — line: identification

1. Introduction

The first study of molecules in the optical spectrum of a post-AGB star concerned the presence of C₃ absorption and C₂ emission in the reflected light of the lobes of the Cygnus Egg Nebula (Crampton et al. 1975). Renewed interest was triggered by the discovery by Waelkens et al. (1992), Balm & Jura (1992), and Hall et al. (1992) of CH⁺ emission in the optical spectrum of the famous Red Rectangle. Recently, Waelkens et al. (1995) reported on the presence of CH⁺ absorption in HD 213985. In this paper (which we will refer to as Paper II) we will study the presence of C₂, CN, and CH⁺ in the optical spectrum of thirteen (post-)AGB stars.

Bakker et al. (1996c, Paper I) were the first to analyze the molecular bands of C₂ and CN in the spectrum of the post-AGB star HD 56126 and showed that the expansion velocity and the excitation conditions are consistent with the lines being formed in the AGB ejecta. Extending this work, Bakker et al. (1995) showed that the same is valid for the molecular absorption lines in four other post-AGB stars (IRAS 04296+3429, IRAS 05113+1347, IRAS 08005-2356, and AFGL 2688) and argued on the

Send offprint requests to: Eric J. Bakker at the University of Texas, ebakker@viking.as.utexas.edu

★ Based on observations with the Utrecht Echelle Spectrograph on the William Herschel Telescope (La Palma, Spain), and the McDonald observatory 2.7m telescope (Texas).

★★ Tables 5 and A.1/2/3/4/5 are available in electronic form at the CDS via anonymous ftp to cdsarc.u-strasbg.fr (130.79.128.5) or via <http://cdsweb.u-strasbg.fr/Abstract.html>, or from the authors.

basis of the relation between CO (or OH for IRAS 08005-2356) and C₂ or CN expansion velocity that these molecular absorption lines are formed in the AGB ejecta and are therefore of circumstellar origin. Hrivnak (1995) discussed the presence of C₂ and C₃ in the low-resolution spectra of nine post-AGB stars.

Theoretical models of the formation and dissociation of molecules in the extended envelope of the carbon-rich AGB star IRC +10216 by Cherchneff et al. (1993) showed that, e.g., C₂ and CN are only present in a thin shell of material within the extended envelope. Close to the star carbon and nitrogen are locked up in complex stable molecules such as C₂H₂ and HCN, while at larger distances the interstellar ultraviolet radiation field photodissociates these molecules to C₂ and CN. At even larger distances the UV radiation field photodissociates simple molecules into their constituent atoms and ions. The net effect is that simple molecules exist only in a thin shell of material.

Interstellar C₂ has been discussed extensively by van Dishoeck & Black (1982). They have shown that the excitation of C₂ is a sensitive balance between photoexcitation and collisional (de-)excitation. By modeling the excitation, the relative population over the rotational energy levels of the C₂ ground state can be used to determine the particle density, radiation field, and kinetic temperature of the line-forming region. In a separate paper (Paper III in preparation) we will apply this model to the stars studied, while an earlier account of this work can be found in Bakker et al. (1995).

In § 2 we discuss the criteria used in selecting our sample of mainly carbon-rich post-AGB stars, and describe the observations and data reduction. § 3 describes the method used in identifying molecular bands and determination of the expansion velocities of the AGB ejecta. Rotational diagrams are used to derive molecular rotational temperatures, column densities, and mass-loss rates. The results are discussed (§ 4) for the sample as a whole and for each star separately. We will finish with a short conclusion (§ 5).

2. Observations and data reduction

2.1. Selection of program stars

After the serendipitous discovery of C₂ and CN in the optical spectrum of HD 56126 (Paper I) we started an extensive observing campaign in order to find additional post-AGB stars with molecular absorption or emission lines. Assuming that the presence of carbon-based molecules is related to the high carbon abundance of the AGB ejecta, we have selected those stars with a carbon-rich circumstellar environment. The presence of the 3.3 and 3.4-3.5 μ m Polycyclic Aromatic Hydrocarbon (PAH) features and of the unidentified 21 μ m feature (Kwok et al. 1989) were used as criteria for the carbon-rich nature of

the AGB ejecta (Table 1). Recently the number of objects exhibiting the 21 μ m feature has been extended (e.g., Henning et al. 1996, Justtanont et al. 1996), and these objects have been selected for a follow-up study. The sample was supplemented with those stars of special importance for the theory of post-AGB evolution (e.g., the metal-depleted post-AGB binaries: HD 52961, HR 4049, BD +39°4926, Red Rectangle, and HD 213985). Two O-rich post-AGB stars (e.g., HD 161796 and IRAS 08005-2356) were added to see whether O-rich stars have the carbon based molecules, and the well studied carbon star IRC+10216 was added to the list, since its spectrum could possibly be used as a template for identifying molecular features. With a limiting magnitude of $m_v = 14$ this resulted in a list of sixteen Post-AGB stars (and IRC +10216) observable from La Palma. IRAS 05341+0852 was added to the list at a later stage. The optical spectrum and the molecular bands are described by Reddy et al. (1997).

The observed stars are listed in Table 1, and the resulting spectra in three selected windows are presented in Figs. 1, 2, and 3. To facilitate comparison **all** velocities given are heliocentric (marked with the symbol v_{\odot}) and the corrections were obtained with the Starlink RV utility Version 2.2.

2.2. Observations and data reduction

2.2.1. WHT/UES

The observations were made in four different runs between February 1992 and August 1994 with the Utrecht Echelle Spectrograph (UES) mounted on the Nasmyth platform of the 4.2m William Herschel Telescope (WHT) on La Palma. The echellograms of February 1992 were recorded on an EEV CCD-05-30 detector with 1242×1152 pixels of $22.5 \times 22.5 \mu\text{m}^2$ each, while in 1994 a Tektronix TK1024A device was used with 1024×1024 pixels of $24 \times 24 \mu\text{m}^2$ each. The wavelength coverage of the UES ranges from 3000 to 11000 Å, and even using the echelle with 31.6 lines per mm, one needs several settings because of the small frame size of the CCD's. For our observations we used settings with central wavelengths of 4020, 5261 and 7127 Å, giving a wavelength coverage from about 3650 to 10000 Å, with some overlap. For each setting Tungsten flatfield and Thorium-Argon (Th-Ar) calibration exposures were taken.

The echellograms from the UES were reduced by TS using the echelle package of IRAF V2.9 running on a DEC3100 workstation. All frames were bias corrected using the overscan columns of the CCD's. The traced orders were extracted with the optimal extraction method using a variance weighting algorithm. Subsequently, the extracted spectra were divided by the identically extracted flatfields and normalized to the continuum. The wavelength calibration was performed using the FIGARO list of Th-Ar

Table 1. Infrared fluxes and spectral features of the seventeen program stars.

Object	Sp.T.	m_v	f_{12} [Jy]	f_{25} [Jy]	3.3 *	3.4-3.5 *	21 *	Remark
IRAS 04296+3429	G0 Ia	14.21	12.74	45.94	e	e	e	...
IRAS 05113+1347	G8 Ia	14.40	3.78	15.30	e	nd	e	...
IRAS 05341+0852	F4 I	12.8	4.51	9.85	e	e	e	s-process enhanced
HD 44179	B9 I	8.84	421.60	456.10	e	nd	nd	IRAS 06176-1036; Red Rectangle
HD 52961	F8 I	8.50	4.53	2.22	no	no	nd	IRAS 07008+1050
HD 56126	F5 I	8.23	24.51	116.70	e	nd	e	IRAS 07134+1005
IRAS 08005-2356	F5 I	11.46	17.96	51.80	no	no	nd	OH maser
IRC +10216	C9.5	11.00	47530.00	23070.00	no	no	nd	IRAS 09452+1330 (carbon star)
HR 4049	F1 I	5.52	48.25	9.55	e	nd	nd	IRAS 10158-2844
HD 161796	F3 Ib	7.27	6.12	183.50	no	no	nd	IRAS 17436+5003 (oxygen rich)
IRAS 20000+3239	G8 Ia	13.40	15.03	70.97	no	no	e	...
AFGL 2688	F5 Iae	14.00	339.00	3041.00	e	no	e	Egg Nebulae
IRAS 22223+4327	G0 Ia	13.30	2.12	37.10	no	e	e	...
HD 235858	G2 Ia	9.30	73.88	302.40	e	e	e	IRAS 22272+5435
HD 213985	B9 I	8.83	5.57	4.66	te	nd	nd	IRAS 22327-1731
BD +39°4926	F1 I	9.24	nd	nd	no	no	no	...
IRAS 23304+6147	G2 Ia	13.15	11.36	59.07	no	no	e	...

*: e: emission; nd: not detected; no: not observed, 3.3, 3.4-3.5, and 21 μm infrared features

lines. About 700 calibration lines, evenly distributed over the orders, were used in a two-dimensional fit with typical rms residuals of 0.25 km s⁻¹ (about 0.1 pixel). By checking the wavelength of a number of telluric oxygen absorption lines, the drift between calibration and target frames was found to be less than 1 km s⁻¹.

The resolution was determined from a number of identified telluric lines (Moore et al. 1966) yielding a *FWHM* of the line profile of 6.0 ± 1.0 km s⁻¹ and a spectral resolving power of $R \sim 5 \times 10^4$. The typical signal-to-noise ratio is $SNR = 100$, and the minimum equivalent width detectable is about 7 mÅ (see App. A only at CDS).

2.2.2. McDonald/CS21

In search for the CH⁺ band towards HD 56126 (no such band was detected), we have obtained high-resolution spectra using the 2DCOUDÉ (CS21) spectrograph (Tull et al. 1995) of the 2.7m telescope at the McDonald observatory. Light was fed to the TK3 CCD, 2048 × 2048 pixels with each $24 \times 24 \mu\text{m}^2$, at the F1 focus using E2 echelle having 52.6759 grooves mm⁻¹. The spectra were reduced by EJB using the data reduction package IRAF: bias and scattered light subtracted, flat fielded and wavelength calibrated using a ThAr arc spectrum. The wavelength calibration has a rms internal error of 0.42 mÅ which corresponds to 0.016 km s⁻¹ at the wavelength of interest. The resolution was determined from the Thorium lines as $R \sim 160,000$.

3. Molecular absorption and emission lines

Table 2. Circumstellar molecular bands in the optical spectra of post-AGB stars.

Molecule	System	Band	(v' , v'')	λ range [Å]
¹² C ¹² C	Phillips	A ¹ Π _u – X ¹ Σ _g ⁺	(1,0)	10137 10213
¹² C ¹³ C	Phillips	A ¹ Π _u – X ¹ Σ _g ⁺	(1,0)	10166 10242
¹² C ¹² C	Phillips	A ¹ Π _u – X ¹ Σ _g ⁺	(2,0)	8753 8913
¹² C ¹³ C	Phillips	A ¹ Π _u – X ¹ Σ _g ⁺	(2,0)	8797 8957
¹² C ¹² C	Phillips	A ¹ Π _u – X ¹ Σ _g ⁺	(3,0)	7717 7809
¹² C ¹³ C	Phillips	A ¹ Π _u – X ¹ Σ _g ⁺	(3,0)	7769 7861
¹² C ¹² C	Phillips	A ¹ Π _u – X ¹ Σ _g ⁺	(4,0)	7910 7002
¹² C ¹³ C	Phillips	A ¹ Π _u – X ¹ Σ _g ⁺	(4,0)	7965 7057
¹² C ¹² C	Swan	d ³ Π _g – a ³ Π _u	(0,0)	5100 5166
¹² C ¹³ C	Swan	d ³ Π _g – a ³ Π _u	(0,0)	5995 5161
¹² C ¹² C	Swan	d ³ Π _g – a ³ Π _u	(1,0)	4710 4740
¹² C ¹³ C	Swan	d ³ Π _g – a ³ Π _u	(1,0)	4705 4735
¹² C ¹⁴ N	Red System	A ² Π – X ² Σ ⁺	(1,0)	9130 9220
¹³ C ¹⁴ N	Red System	A ² Π – X ² Σ ⁺	(1,0)	9159 9249
¹² C ¹⁴ N	Red System	A ² Π – X ² Σ ⁺	(2,0)	7874 7918
¹³ C ¹⁴ N	Red System	A ² Π – X ² Σ ⁺	(2,0)	7918 7962
¹² C ¹⁴ N	Red System	A ² Π – X ² Σ ⁺	(3,0)	6927 6954
¹³ C ¹⁴ N	Red System	A ² Π – X ² Σ ⁺	(3,0)	6967 6994
¹² C ¹⁴ N	Red System	A ² Π – X ² Σ ⁺	(4,0)	6190 6225
¹³ C ¹⁴ N	Red System	A ² Π – X ² Σ ⁺	(4,0)	6244 6279
¹² C ¹ H ⁺		A ¹ Π – X ¹ Σ ⁺	(0,0)	4220 4280
¹³ C ¹ H ⁺		A ¹ Π – X ¹ Σ ⁺	(0,0)	4220 4280
¹² C ¹ H ⁺		A ¹ Π – X ¹ Σ ⁺	(1,0)	3950 3990
¹³ C ¹ H ⁺		A ¹ Π – X ¹ Σ ⁺	(1,0)	3950 3990

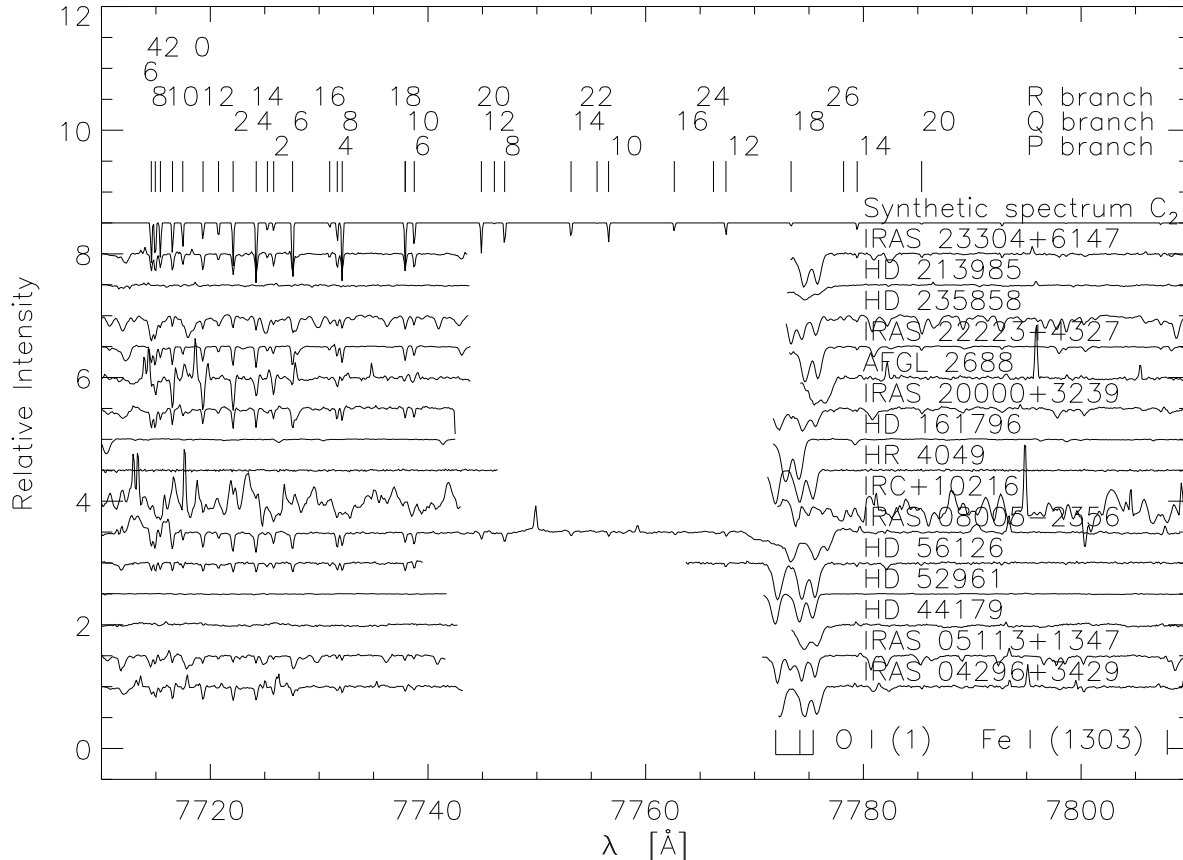


Fig. 1. Spectra of the observed stars in the wavelength region of the C₂ A¹Π_u – X¹Σ_g⁺ (3,0) band. The top spectrum is a synthetic spectrum computed using $T_{\text{rot}} = 200$ K, $\log N = 15.60$ cm⁻² and $R \sim 5 \times 10^4$. All other spectra are corrected for the velocity of the molecular lines such that the molecular lines are at their rest wavelengths. The three absorption lines near 7775 Å are due to the OI(1) multiplet. Note that the wavelength part from 7740 Å to 7770 Å is not observed for most of the objects in the sample.

3.1. Identification of molecular bands

Molecular absorption line profiles resemble closely those of telluric absorption lines, while molecular emission line profiles can easily be confused with cosmic spikes. To prevent confusion with cosmic spikes most integrations were divided into two or more shorter exposures, and the individual spectra were combined after the reduction process using a median filter to remove cosmic spikes. A number of (hot) stars have been observed to identify telluric lines.

In this paper we have restricted ourselves to twelve molecular bands and their ¹³C isotopic species (Table 2) of three different species (C₂, CN, and CH⁺). Table 3 gives for each star observed and for each molecular band, whether it was detected (in absorption or emission), tentatively detected (mostly when the lines are severely blended by photospheric lines), or not detected at all. We have carefully studied all spectra to find ad-

ditional “prominent” molecular bands, but none were detected. Of course this does not exclude the presence of weak molecular bands with equivalent widths of less than 10 mÅ. IRAS 05113+1347, IRAS 20000+3239, and HD 235858 show also CN Red System band photospheric absorption (Fig. 2). These lines are easily distinguishable from the circumstellar CN lines, since the lines are much broader and they are identified with much higher energy levels (typically $30 \leq N'' \leq 90$).

We have carefully looked for the isotopic lines, e.g., ¹²C¹³C, ¹³C¹⁴N, and ¹³CH⁺, with negative results. From this we deduce a typical lower limit on the isotope ratio of ¹²C/¹³C > 20.

In Paper I we pointed out that optical depth effects play an important role for the stronger molecular bands; therefore in this study we have limited the analysis to the weaker molecular bands: C₂ Phillips (3,0) (Fig. 1), CN Red System (3,0) (Fig. 2), and CH⁺ (0,0) (Fig. 3).

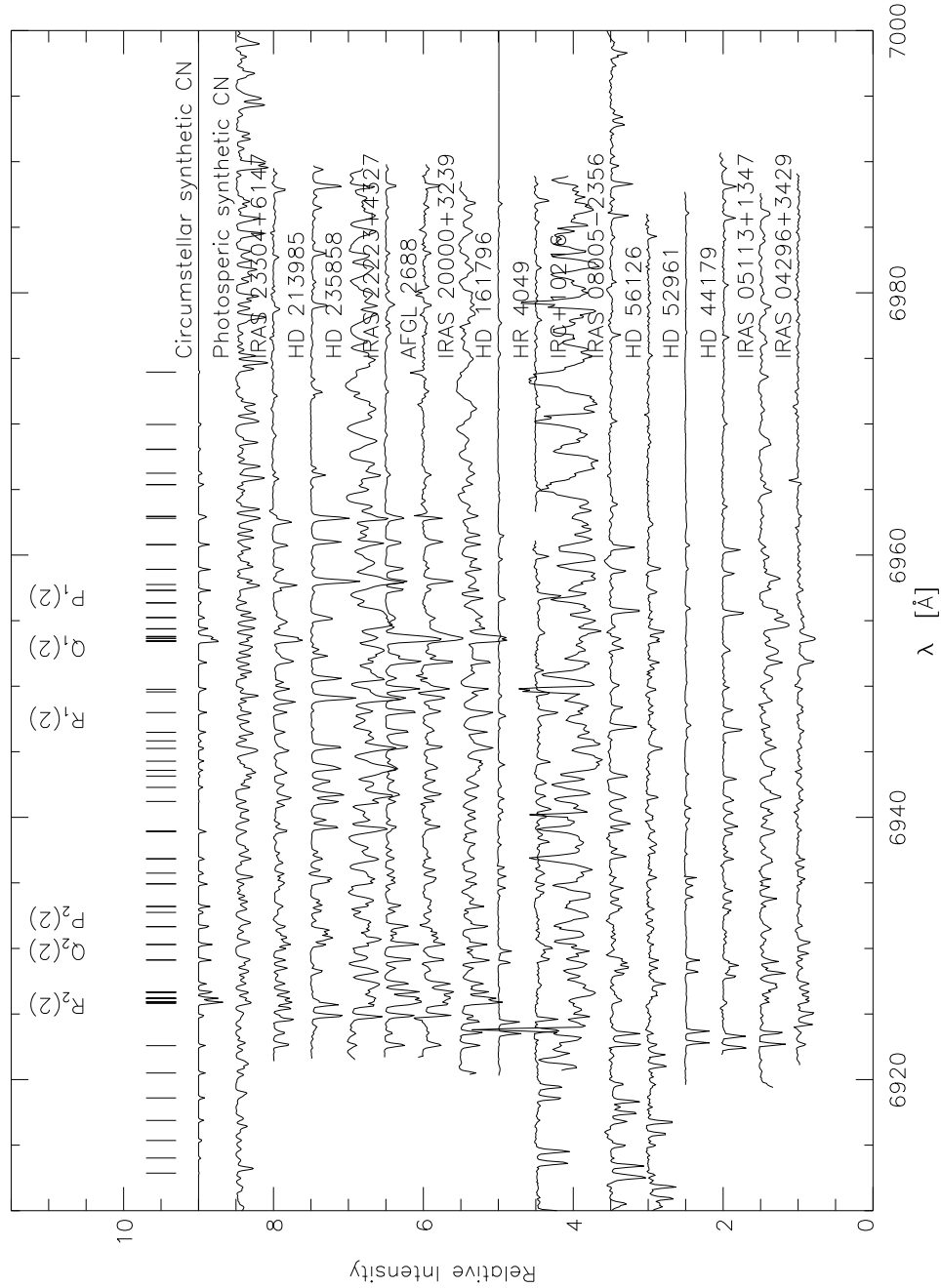


Fig. 2. Spectra of the observed stars in the wavelength region of the CN $A^2\Pi - X^2\Sigma^+$ (3,0) band. The top spectrum is a synthetic spectrum of circumstellar ^{12}CN computed using $T_{\text{rot}} = 25$ K, $\log N = 16.50 \text{ cm}^{-2}$ and $R \sim 5 \times 10^4$, followed by a synthetic spectrum of photospheric ^{12}CN using $T_{\text{rot}} = 5500$ K and $\log N = 16.78 \text{ cm}^{-2}$. All spectra are corrected for the velocity of the molecular lines such that the circumstellar molecular lines are at their rest wavelengths. Most of the unidentified narrow absorption lines (see HR 4049 which has no circumstellar or photospheric lines in this part of the spectrum) are due to telluric O₂ and H₂O (Moore et al. 1966) or photospheric CN (only for HD 235858, IRAS 20000+3239, and IRAS 05113+13477).

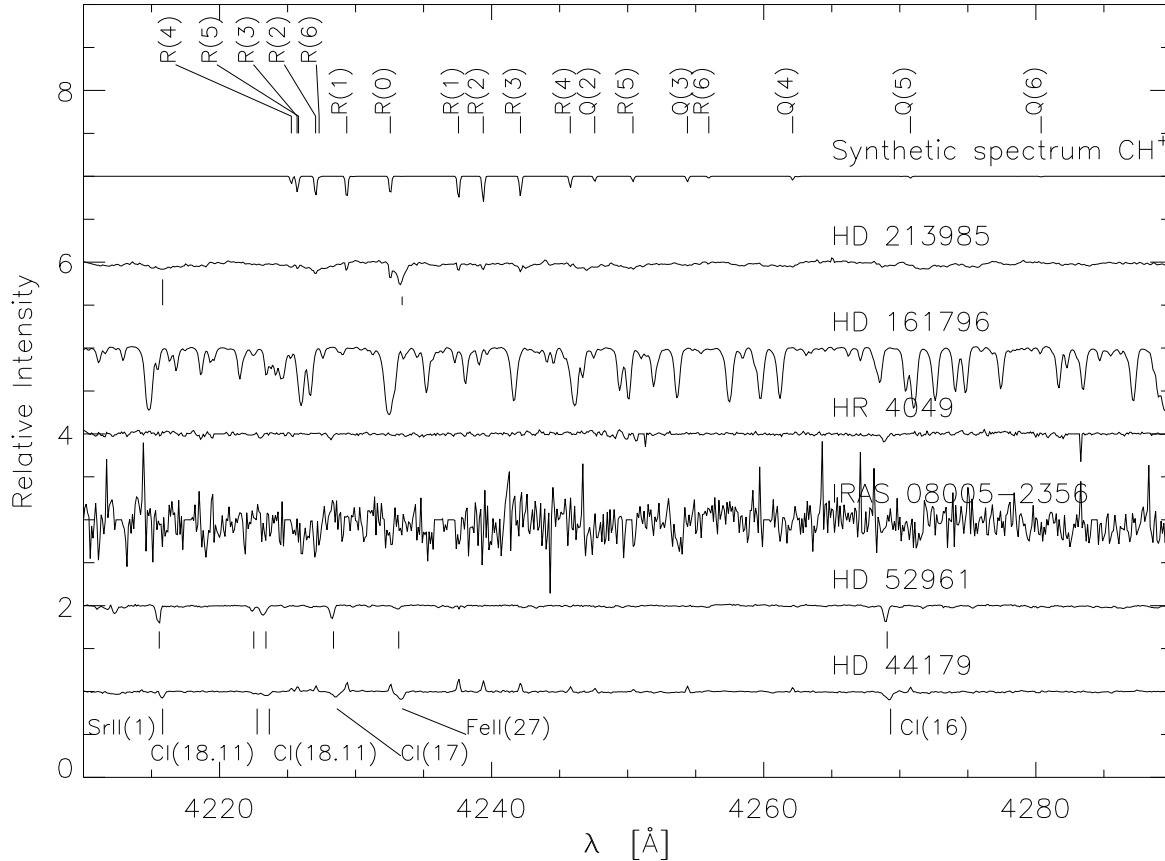


Fig. 3. Spectra of the observed stars in the wavelength region of the CH⁺ A¹Π – X¹Σ⁺ (0,0) band. The top spectrum is a synthetic spectrum computed using $T_{\text{rot}} = 200$ K, $\log N = 14.70$ cm⁻² and $R = 5 \times 10^4$. All other spectra are corrected for the velocity of the molecular lines such that the molecular lines are at their rest wavelengths. Note the broad photospheric absorption features in the spectrum of HD 213985 (e.g., SrII(1) and the somewhat narrower FeII(27) feature.)

The wavenumbers of the C₂ Phillips bands have been taken from Chauville et al. (1977) ((1,0) and (2,0)) and Ballik & Ramsay (1963) (3,0) and CH⁺ (0,0) and (1,0) bands from Carrington & Ramsay (1982). Conversion from wavenumber in vacuum to wavelength in air was made by applying Cauchy’s formula. Wavelengths of the CN Red System were extracted from the SCAN tape (Jørgenson & Larsson 1990).

3.2. Determination of the expansion velocity, rotational temperature, column density, time-scale, and mass-loss rate

3.2.1. Expansion velocity

The first step in analyzing a molecular band is to check that all the candidate molecular lines yield the same radial velocity. The average radial velocity of all lines is a good measure for the true velocity of the line-forming region.

For absorption lines this is the line-of-sight to the star, while for emission lines it can be anywhere within the “slit” (defined as the area on the CCD used for extracting the spectrum) of the telescope.

In Paper I we showed that the molecular absorption lines in the spectrum of HD 56126 are formed in the AGB ejecta. Now we investigate for the current sample if there is a correlation between the expansion velocities of the AGB ejecta derived from CO (or OH for IRAS 08005-2356) emission line profiles, and the velocity differences between the molecular absorption lines and the system velocities. The system velocity was taken to be the central velocity of the CO or OH line emission profile or from radial velocity studies on binaries (Table 4). The velocities of the photospheric lines are not a good estimate of the system velocity, since most of the star in the sample are somewhat pulsating and/or are binaries.

The upper panel of Fig. 4 shows that the expansion velocity derived from CO or OH emission lines and those de-

Table 3. The detection of molecular bands in the optical spectra of post-AGB stars.

Object	C ₂ Swan *		C ₂ Phillips*			CN Red System *				CH ⁺ *	
	d ³ Π _g – a ³ Π _u		A ¹ Π _u – X ¹ Σ _g ⁺			A ² Π – X ² Σ ⁺				A ¹ Π – X ¹ Σ ⁺	
	(0,0)	(1,0)	(1,0)	(2,0)	(3,0)	(1,0)	(2,0)	(3,0)	(4,0)	(0,0)	(1,0)
IRAS 04296+3429	no	no	a	a	a	a	a	a	b	no	no
IRAS 05113+1347	a	b	a	a	a	a	a	a	b	no	no
IRAS 05341+0852	no	no	a	a	a	a	a	a	no	no	no
HD 44179	np	np	np	np	np	np	np	np	np	e	e
HD 52961	np	np	np	np	np	np	np	np	np	np	np
HD 56126	a	a	a	a	a	a	a	a	a	np	np
IRAS 08005-2356	ta	no	a	a	a	a	a	np	np	b	b
IRC +10216	b	b	a	a	a	a	ta	b	b	no	no
HR 4049	np	np	np	np	np	np	np	np	np	np	np
HD 161796	no	no	np	np	np	np	np	np	np	np	np
IRAS 20000+3239	a	b	no	a	a	a	a	a	a	no	no
AFGL 2688	a	b	e	a	a	a	a	a	a	no	no
IRAS 22223+4327	a	a	no	a	a	a	a	a	a	no	no
HD 235858	a	a	a	a	a	a	a	b	b	no	no
HD 213985	np	np	np	np	np	np	np	np	np	a	a
BD +39°4926	no	no	no	no	no	no	no	no	no	np	no
IRAS 23304+6147	a	a	no	a	a	a	a	a	a	no	no

* a: absorption; b: blended; e: emission; no: not observed; np: not present; ta: tentative absorption
C is ¹²C, N is ¹⁴N, and H is ¹H

Table 4. Adopted system and AGB outflow velocities of programs stars.

Object	$v_{\text{sys,lsr}}$ ^a	$v_{\text{sys},\odot}$ ^b	v_{exp} ^c	Remark	Reference
IRAS 04296+3429	−66.0	−59.0	12.0	CO($J = 2 - 1$)	O
IRAS 05113+1347	−12.0	2.0	...	photospheric lines	B
IRAS 05341+0852	9.6	25.0	...	photospheric lines	R
HD 44179	2.7	20.7	6.0	binary $P = 310 \pm 3$ days	V,J
HD 52961	pulsator $P = 70.8$ days	F
HD 56126	71.0	85.6	10.0	CO	Z
IRAS 08005-2356	46.7	61.1	49.8	OH maser	T
IRC +10216	−26.2	−19.1	14.1	pulsator $P = 638$ days	H,D
HR 4049	−44.5	−32.9	...	binary $P = 429$ days	V
HD 161796	−36.0	−0.4	11.5	CO($J = 1 - 0$)	L
IRAS 20000+3239	14.0	−4.1	12	CO($J = 1 - 0$)	O
AFGL 2688	−33.3	−49.2	22.8	...	Y
IRAS 22223+4327	−30.0	−42.2	14.0	CO($1 - 0$)	O
HD 235858	−30.9	−43.1	11.6	CO	Z
HD 213985	−42.5	−45.7	...	binary $P = 259$ days	V
BD +39°4926	binary $P = 775$ days, no infrared excess	K
IRAS 23304+6147	−15.9	−25.8	15.5	CO($2 - 1$)	W

^a v_{lsr} is the system velocity in the local standard of rest system [km s^{−1}]

^b v_{\odot} is the system velocity in the heliocentric system [km s^{−1}]

^c v_{exp} the expansion velocity of the AGB ejecta [km s^{−1}]

B: this study; D: Dyck et al 1991; F: Fernie 1995; H: Huggins et al. 1988; K: Kodaira et al. 1970; J: Jura et al. 1995; L: Likkell et al. 1987; O: Omont et al. 1993; R: Reddy et al. 1997; T: Te Lintel Hekkert et al. 1991; V: van Winckel et al. 1995; W: Woodsworth et al. 1990; Y: Young et al. 1992; Z: Zuckerman et al. 1986

Table 5. Physical parameters derived from the molecular lines.

Object	C ₂ A ¹ Π _u – X ¹ Σ _g ⁺ (3,0) or (2,0) ^a					CN A ² Π – X ² Σ ⁺ (2,0) or (3,0) ^b					δv ^e	$\frac{N(\text{CN})}{N(\text{C}_2)}$	¹² C/ ¹³ C
	v_{\odot} [km s ⁻¹]	v_{exp}^c [km s ⁻¹] ±2.0	T_{rot} [K]	$\log N_{\text{mol}}^d$ [cm ⁻²] ±0.10	$\log \dot{M}$ [M _⊙ yr ⁻¹] ±1	v_{\odot} [km s ⁻¹]	v_{exp}^c [km s ⁻¹] ±2.0	T_{rot} [K]	$\log N_{\text{mol}}^d$ [cm ⁻²] ±0.10	$\log \dot{M}$ [M _⊙ yr ⁻¹] ±1			
IRAS 04296+3429	-66.7 ± 0.4	7.7	138 ± 14	15.21(15.20)	-5.8	-63.6 ± 0.6	4.6	25 ± 06	15.91	-5.2	-3.1 ± 0.8	4.9	≥ 20
IRAS 05113+1347	-2.5 ± 0.6	4.5	198 ± 31	15.13(15.13)	-6.1	-3.6 ± 1.1	5.6	19 ± 02	15.89	-5.1	1.1 ± 1.3	5.6	≥ 20
IRAS 05341+0852	13.4 ± 0.8	11.6	77 ± 09	15.00(14.61)	-6.0	15.0 ± 0.4	10.0	38 ± 04	15.86	-5.0	-1.6 ± 1.0	7.2	...
HD 56126	77.3 ± 0.1	8.3	242 ± 34	15.31(15.28)	-5.5	78.3 ± 0.2	7.3	25 ± 08	15.51	-5.2	-1.0 ± 0.2	1.5	≥ 20
IRAS 08005-2356	17.4 ± 0.4	43.7	149 ± 10	15.55(15.60)	-4.7	22.3 ± 0.2	42.2	38 ± 02	15.48	-4.7	-4.9 ± 0.4	0.8	≥ 11
IRC +10216	-33.3 ± 0.7	14.2	43 ± 16	14.90(15.15)	-6.3	-33.8 ± 0.5	14.7	28 ± 05	15.03	-6.0	-0.5 ± 0.9	1.5	...
IRAS 20000+3239	-16.9 ± 0.4	12.8	234 ± 33	15.41(15.44)	-5.3	-17.0 ± 0.3	12.9	50 ± 02	16.47	-4.1	0.1 ± 0.5	11.2	≥ 20
AFGL 2688	-66.5 ± 0.3	17.3	56 ± 08	15.47(15.51)	-4.8	-64.5 ± 0.5	15.3	18 ± 03	16.10	-4.1	-2.0 ± 0.6	4.2	≥ 19
IRAS 22223+4327	-57.2 ± 0.2	15.0	399 ± 36	15.57(15.55)	-4.6	-55.0 ± 0.3	12.8	30 ± 04	16.34	-3.8	-2.2 ± 0.4	5.8	≥ 20
HD 235858	-52.2 ± 0.3	9.1	119 ± 35	15.20(15.27)	-5.7	-51.8 ± 0.1	8.7	24 ± 17	15.03	-5.8	-0.4 ± 0.3	0.6	≥ 11
IRAS 23304+6147	-39.7 ± 0.3	13.9	281 ± 21	15.57(15.57)	-5.0	-39.2 ± 0.5	13.4	43 ± 14	16.17	-4.3	-0.5 ± 0.6	3.8	≥ 20
CH ⁺ A ¹ Π – X ¹ Σ ⁺ (0,0)													
HD 44179 ^f	17.3 ± 0.5	3.4	202 ± 16	14.44(14.49)	≥ 22
HD 213985	-52.4 ± 0.6	6.7	155 ± 22	14.35(14.35)	≥ 38

^a C₂ (2,0) for IRC +10216, else C₂ (3,0)^b CN (2,0) for IRAS 08005-2356, HD 235858, and IRC +10216, else CN (3,0)^c $v_{\text{exp}} = v_{\text{sys}} - v_{\text{C}_2/\text{CN}/\text{CH}^+}$ ^d in brackets: sum over J'' or N'' levels of observed transitions^e $\delta v = v_{\text{CN}} - v_{\text{C}_2}$ ^f the emission line spectrum has been analyzed with A¹Π $J' = 0$ as energy zerolevel. v_{exp} and T_{rot} are real, but the column density of HD 44179 is rather meaningless

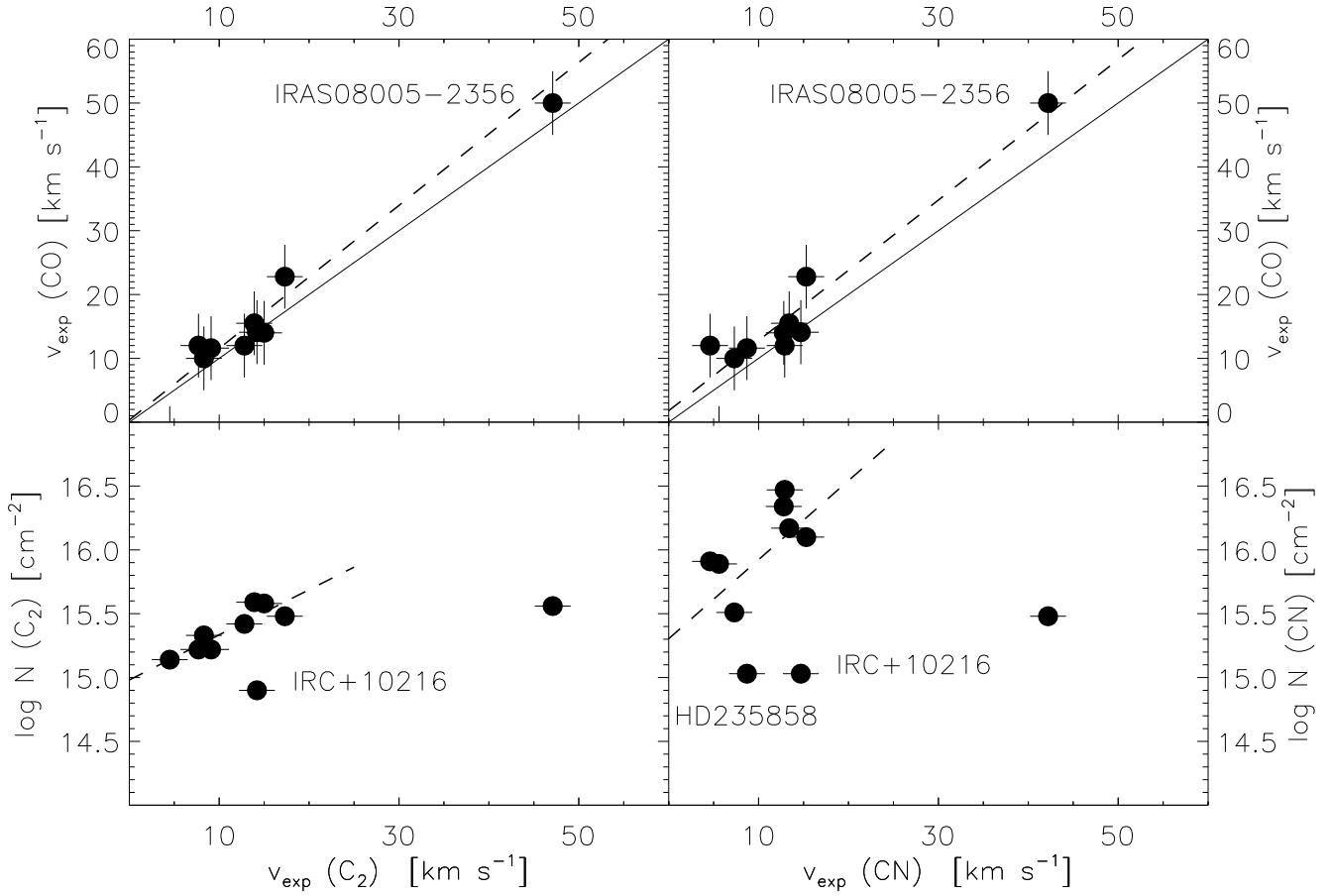


Fig. 4. Top panels: expansion velocities derived from CO (or OH for IRAS 08005-2356) versus expansion velocities derived from C₂ and CN. Lower panels: C₂ and CN column density versus C₂ and CN expansion velocity. The solid lines in the upper two panels give the relations in which the two velocities are equal. The dashed lines are linear least-squares fits as given in the text. IRAS 05341+0852 is not plotted.

rived from C₂ or CN absorption lines are identical within the estimated error of 2 km s⁻¹. The expansion velocities determined from C₂, CN, CH⁺ are tabulated in Table 5. This proves unambiguously that the line-forming region of these molecular absorption lines is the AGB ejecta (circumstellar shell). The optical molecular lines are not resolved ($FWHM \sim 6.0$ km s⁻¹), which puts an upper limit of 6.0 km s⁻¹ on the turbulent broadening and velocity stratification within the line-forming region. The CH⁺ detections are discussed in §4, but to first order they have the same range of expansion velocities. A linear least-squares fit (excluding IRAS 05113+1347, IRAS 05341+0852 for which no CO data are available) gives:

$$v_{\text{exp}}(\text{CO}) = 1.12 \times v_{\text{exp}}(\text{C}_2) + 0.36 \quad (1)$$

$$v_{\text{exp}}(\text{CO}) = 1.10 \times v_{\text{exp}}(\text{CN}) + 1.80 \quad (2)$$

with correlation coefficients of 0.98 and 0.97, respectively. All velocities are in units of km s⁻¹.

3.2.2. Rotational temperature and molecular column density

The second step is to determine the equivalent widths of the lines and to construct rotational diagrams (Fig. 5, 6, 7, and 8). All rest wavelengths, (absorption) oscillator strengths and equivalent widths of the lines used are tabulated in App. A (available only at CDS or from the authors). The adopted method is extensively discussed in Paper I, and we refer the interested reader to that paper for all details on the rotational diagram. Unfortunately there is a error in Eq. 5 of Paper I. The correct equation is: $S_{J''}^Q = (2J'' + 1)$ (page 208, Herzberg 1950).

The (absorption) oscillator strengths were computed in the usual way (see Paper I for further references) using band oscillator strengths of $f_{(2,0)} = 1.44 \times 10^{-3}$ and $f_{(3,0)} = 6.672 \times 10^{-4}$ for C₂ Phillips (2,0) and (3,0) band respectively (Langhoff et al. 1990, Langhoff 1996), and $f_{(0,0)} = 5.45 \times 10^{-3}$ for CH⁺ (0,0) (Larsson & Siegbahn

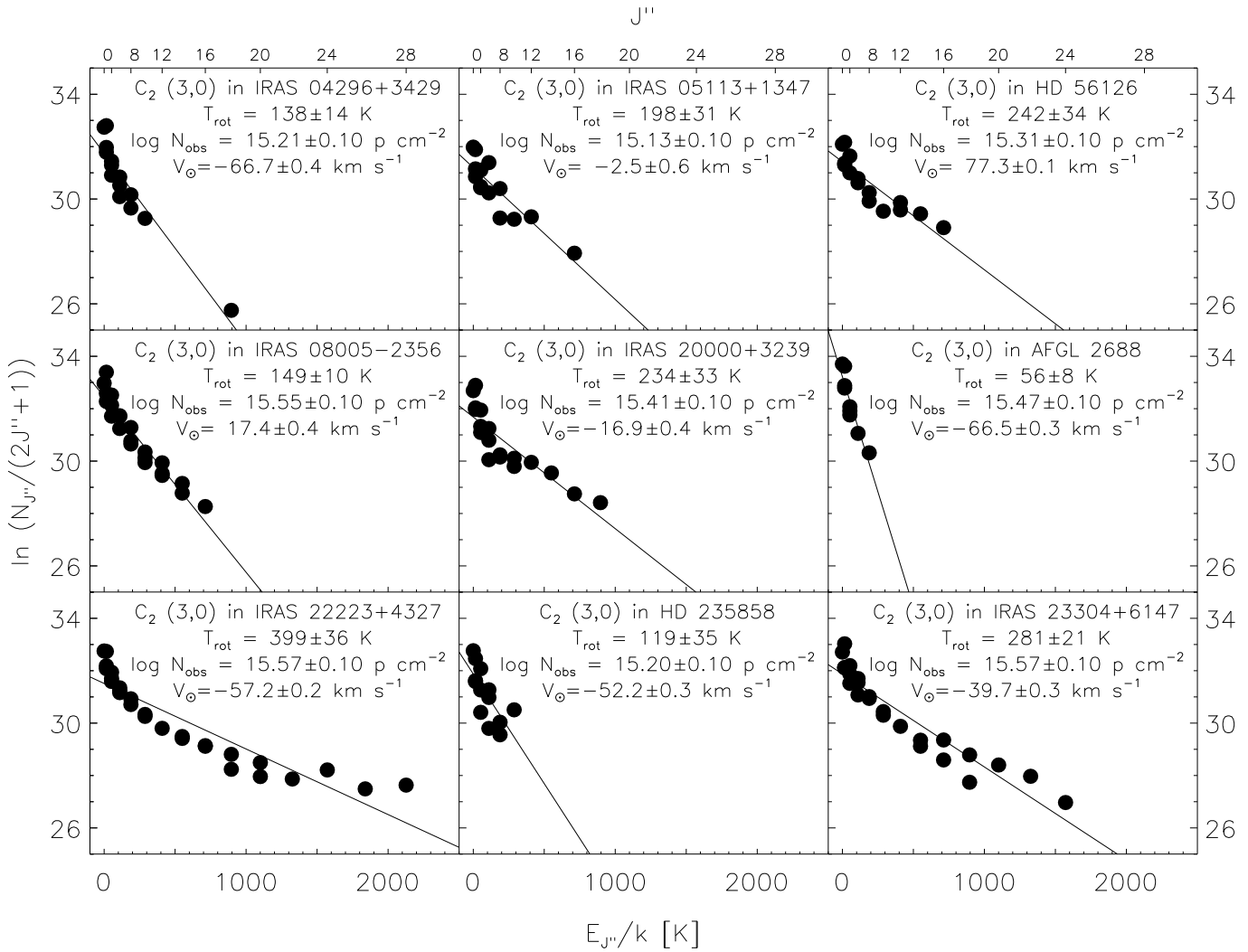


Fig. 5. Rotational diagrams for the stars showing the Phillips C_2 (3,0) absorption. Note that for those stars for which transitions from high J'' levels are observed (e.g., IRAS 22223+4327), the rotational diagram shows a flattening due to optical pumping of the molecule (see §3.2.2 for details).

1983). For CH^+ emission the emission oscillator strength is given by $g_{J'} f_{emission} = g_{J''} f_{absorption}$. All data of the CN Red System were extracted from the SCAN tape of Jørgenson & Larsson (1990) with the oscillator strength multiplied by 0.734 as suggested by the authors.

The rotational temperature is determined using rotational constant, B_v , values of 1.8111, 1.8907, 13.9302, and 11.4227 cm^{-1} for C_2 $X^1\Sigma_g^+ v'' = 0$ (Marenin & Johnson 1970), CN $X^2\Sigma^+ v'' = 0$ (Brocklehurst et al. 1971), CH^+ $X^1\Sigma^+ v'' = 0$ (Carrington & Ramsay 1982) and CH^+ $A^1\Pi v' = 0$ (Carrington & Ramsay 1982), respectively. Higher order corrections terms (e.g. D_v , H_v) where included if needed.

In Paper I we have shown that only the C_2 and CN (3,0) band of HD 56126 are optically thin. In order to facilitate the analysis, we have limited ourself to the C_2 (3,0) and CN (3,0) bands. For each molecular band we inves-

tigated whether the different branches for a given lower level gave the same column density. Within the errors of the determination of the equivalent width this was indeed the case. In case the lines would have been optically thick, this would have shown up as vertical scatter in the rotational diagrams (Fig. 5, and 6). This is not observed, and it confirms that the lines are optically thin.

Recently Bakker et al. (1996d) studied the C_2 and CN bands of HD 56126 by means of a curve of growth analysis. They find that the (3,0) bands are indeed close to being optically thin. However, in this work any errors which are introduced due to the assumption that the lines are optically thin are negligible with respect to the errors in the measurements of the equivalent width.

CH^+ absorption and emission is assumed to be optically thin based on the narrow correlation of the data points in the rotation diagram (Fig. 7), and the fact that

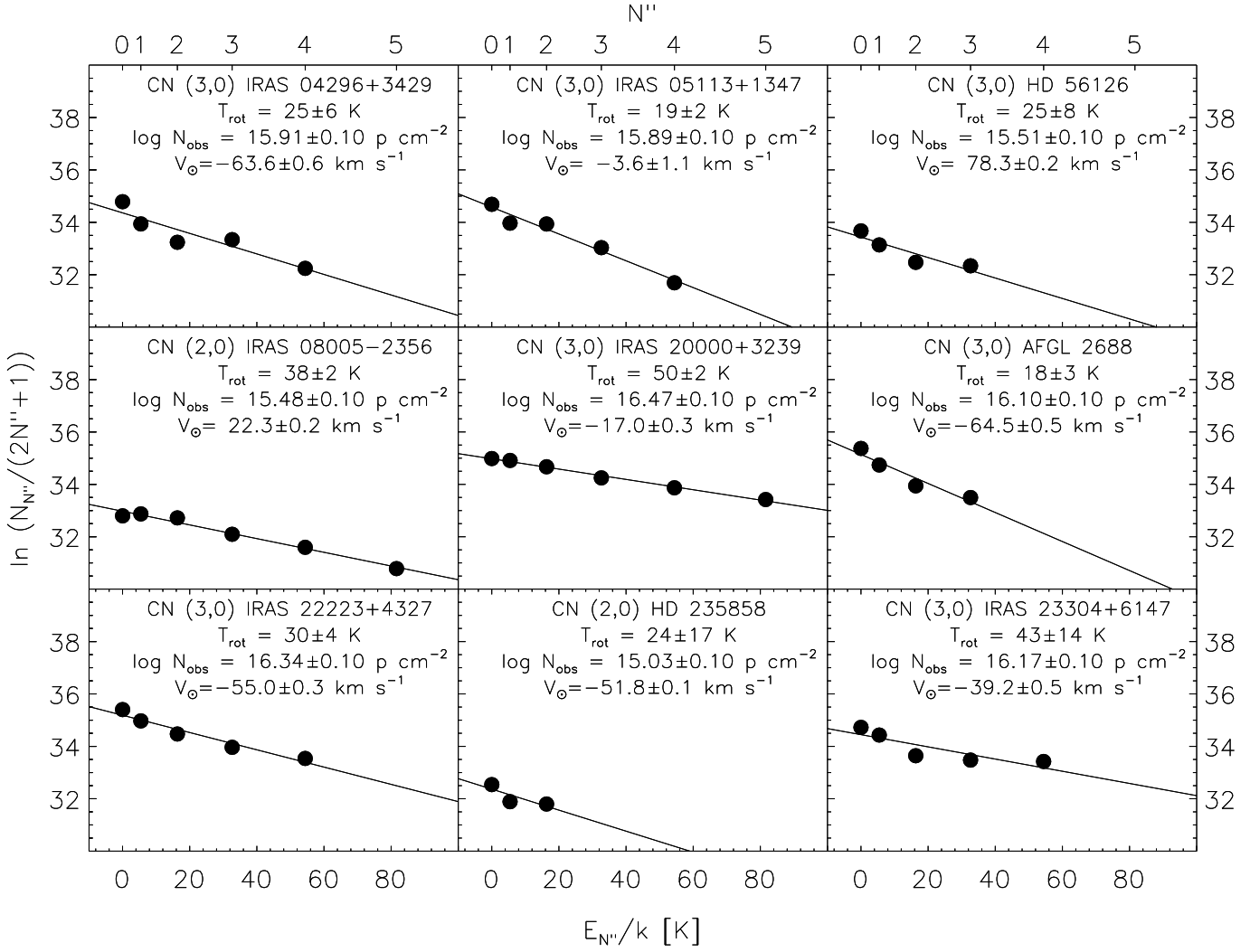


Fig. 6. Rotational diagrams of the CN Red System (3,0) band (if not detected the (2,0) band) for the stars showing CN absorption. Note that the energies have been computed relative to $N'' = 0$.

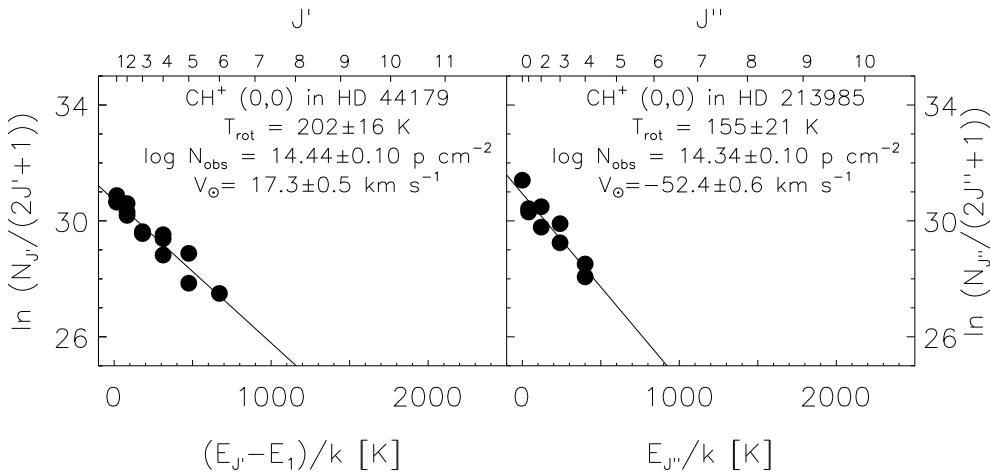


Fig. 7. Rotational diagrams for the stars showing the CH⁺ (0,0) absorption or emission. For CH⁺ emission the energy levels are relative to A¹Π $J' = 1$.

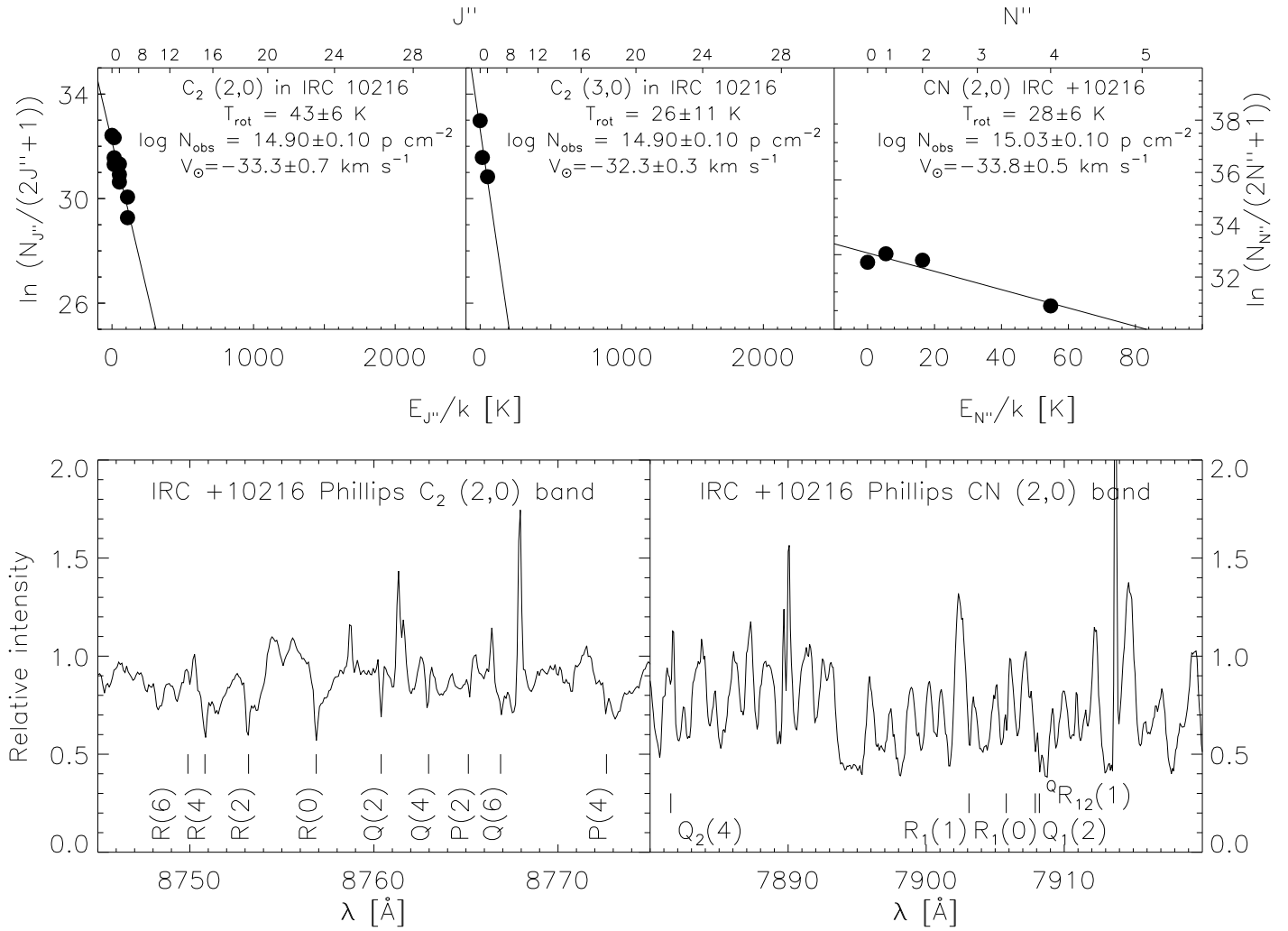


Fig. 8. The rotational diagrams of the C₂ Phillips (2,0) and (3,0) and CN Red System (2,0) absorption bands in the spectrum of IRC +10216. The lower panels give the part of the spectrum on which we have based our firm identification of C₂ and tentative identification of CN (see text for details).

different branches (P, Q, and R) do yield comparable column densities for the J'' (or J') level they originate from. The relative rotational diagram for CH⁺ emission is relative to the energy level of the A¹Π $J' = 1$ level. This energy level is at 42400 K (over forty thousand degrees!) above ground level.

If the population distribution over the rotational levels follows a Boltzmann distribution, then the rotational diagram should be a linear relation for optically thin lines ($\tau \leq 1$). The slope of the curve is inversely proportional to the rotational temperature T_{rot} and the offset is given by the natural logarithm of N_{mol}/Q_r , where N_{mol} is the column density of the molecule and Q_r the partition function. If the rotational temperature is not equal to the kinetic temperature and different for each pair of levels, then the population distribution over the rotational levels is non-Boltzmann and the rotational diagram will be non-linear. From linear least-squares fits to the rotational diagrams, we find typical values of $T_{\text{rot}} = 43 - 399$ K, $\log N_{\text{mol}} = 14.90 - 15.57$ cm⁻² for C₂ (3,0) (or (2,0)),

$T_{\text{rot}} = 155 - 202$ K, $\log N_{\text{mol}} = 14.35$ cm⁻² for CH⁺ (0,0), and $T_{\text{rot}} = 18$ to 50 K, $\log N_{\text{mol}} = 15.03$ to 16.47 cm⁻² for CN (3,0) (or (2,0)) with an average particle ratio of $N(\text{CN})/N(\text{C}_2) = 4.0 \pm 3.0$.

Since the rotational temperature is determined using all available data points, it is an average temperature. For C₂, use of only the low J'' levels (which are most sensitive to collisional (de-)excitation) results in a lower rotational temperature, which will be closer to the kinetic temperature of the gas. On the other hand, using only the high- J'' levels (which are sensitive to radiative pumping) results in a rotational temperature which will be closer to the color temperature of the exciting stellar radiation field.

The column densities are computed using the partition function, which depends on the average rotational temperature. In Paper I we investigated the accuracy of this method and found that the column densities are slightly underestimated for super-thermal C₂, and slightly overestimated for sub-thermal CN. This introduces a relative error of about 10%. A slightly more accurate determina-

tion of the molecular column density could be obtained by adding the column densities of all observed J'' levels and extrapolating to the unobserved levels. The oscillator strengths are not very well known and we adopt an absolute error of 15%. As a consequence, we will adopt an absolute error of 15% and a relative error of 10% to the molecular column densities.

The detection of C₂ and CN in the same spectrum of the same star with significantly different rotational temperatures can be attributed to the difference in the dipole moment of the two molecules. C₂ is a homonuclear molecule (the electronic configuration is spatially symmetric with respect to the rotational axis, and the nuclear spin of ¹²C is $I = 0$). Thus, without a permanent dipole moment the selection criteria forbid pure rotational and rotational-vibrational transitions in the ground electronic state (except through weak quadrupole transitions). A homonuclear molecule has therefore no efficient transitions available to emit a photon. The higher- J'' levels will be overpopulated relative to a Boltzmann distribution at the local kinetic temperature, because they can be populated by radiation with a color temperature larger than the local kinetic temperature (optical pumping). The molecule is super-thermally excited. In Fig. 5 this shows up as a flattening of the curve for $J'' \geq 20$ levels. CN is a heteronuclear molecule and selection criteria allow dipole transitions: energy can be easily released and the molecule cools to sub-thermal values if the density is below the density for collisional excitation.

Remarkably, there seems to be a relation between the molecular column density and the expansion velocity. Since CN can only be photodissociated by far UV photons ($\lambda \leq 1100$ Å), it is more sensitive to the interstellar UV radiation field, this leads to a large spread in the observed CN column densities. A linear least-squares fit (excluding IRAS 08005-2356, IRAS 05341+0852, and IRC 10216) yields:

$$\log N(\text{C}_2) = 3.53 \times 10^{-2} \times v_{\text{exp}}(\text{C}_2) + 14.98 \quad (3)$$

$$\log N(\text{CN}) = 6.19 \times 10^{-2} \times v_{\text{exp}}(\text{CN}) + 15.3 \quad (4)$$

with correlation coefficients of 0.89 and 0.53, respectively. Column densities and velocities are in units of cm⁻² and km s⁻¹ respectively. A detailed discussion of this relation will be given in § 4, where we will argue that it reflects differences in intrinsic carbon abundance.

3.2.3. Time scales of AGB ejecta

The far-infrared radiation (IRAS data) is due to thermal radiation of dust in the AGB ejecta. From the IRAS 12 to 25 μm flux ratio, $f_v(12\mu\text{m})/f_v(25\mu\text{m})$, we derived the color temperature of the innermost dust using the method described in the IRAS Explanatory Supplement (1986) and Table Suppl. VI.C.6. (Table 1). For stars with a near-infrared excess (e.g., a circumbinary disk) this method

cannot be applied, and we cannot calculate the mass-loss rate as described here.

Trams (1991) has fitted an optically thin dust model to a dozen post-AGB stars and found that for all stars the dust emissivity efficiency, $Q(\nu) = Q_0(\nu/\nu_0)^p$, has an index parameter $p = 1$. Following Sopka et al. (1985), the dust inner radius (r_o) is given by:

$$\frac{r_o}{R_*} = \left(\frac{T_{\text{dust}}}{0.6T_{\text{eff}}} \right)^{-\left(\frac{4+p}{2}\right)} \quad (5)$$

with T_{dust} and T_{eff} the Blackbody dust temperature and the stellar effective temperature, respectively. Adopting $\log L_* = 3.86 \log L_\odot$ for a 0.6 M_⊙ post-AGB star (Blöcker 1995) the stellar radius, R_* , can be calculate. Typical distances derived are of the order of 10¹⁶ cm (Table 6). Taking the dust inner radius and the expansion velocity, we can subsequently estimate the time since the star left the AGB (Eq. 6, Table 6) and the average annual increase in effective temperature (Eq. 7, Table 6):

$$t_{\text{post-AGB}} = \frac{r_o}{v_{\text{exp}}} \quad (6)$$

$$\frac{\Delta T}{\Delta t} = \frac{T_{\text{eff}} - T_{\text{AGB}}}{t_{\text{post-AGB}}} \quad (7)$$

while taking $T_{\text{AGB}} = 3500$ K.

The stars in our sample left the AGB typically 300 years ago and they have a typical annual effective temperature increase of 5 K. Since an abundance analysis allows the determination of the effective temperature as accurate as 100 K (for supergiants), this suggests that we expect to see change in the effective temperature and conditions of the molecules on a time scale of about 20 years.

3.2.4. Mass-loss rate

Here we will attempt to derive the mass-loss rates from the column densities and expansion velocities in the AGB ejecta. In order to do so, we will make two important simplifications:

(i) Since there is no simple, unique way to determine the distance from the star to the molecules, we will assume that the molecules reside where dust is present. In the case of the extended envelope of AGB stars and in the circumstellar shells of post-AGB stars (F to G-type stars), simple molecules are formed out of complex molecules by photodissociation by the interstellar radiation field. However, for circumstellar shells the abundance of a simple molecule will peak at a distance larger than the dust inner radius. Therefore, the assumption that the molecules are formed at the dust inner radius and beyond underestimates the derived mass-loss rate.

(ii) Our second assumption is that the molecular abundances are the same for each star, resemble those of the AGB star IRC +10216, and do not change with distance

Table 5. Derived stellar and dust parameters assuming $\log L_* = 3.86 \log L_\odot$.

Object	T_{eff} [K]	R_* [R _⊙]	T_{dust} [K]	r_0 [R _*]	$\log r_0$ [cm]	t [yr]	$\Delta T/\Delta t$ [K yr ⁻¹]	Remark
IRAS 04296+3429	5550	92	195	1200	15.89	320	6	...
IRAS 05113+1347	4600	134	185	860	15.91	570	2	...
IRAS 05341+0852	6500	67	235	1120	15.72	154	19	...
HD 44179	10300	27	320	near-ir excess
HD 56126	6900	60	175	2720	16.06	440	8	...
IRAS 08005-2356	6900	60	210	1730	15.86	50	70	near-ir excess ??
IRC 10216	2200	...	240
IRAS 20000+3239	4600	134	175	990	15.97	330	5	...
AFGL 2688	6900	60	145	4360	16.26	330	10	...
IRAS 22223+4327	5550	92	120	4060	16.42	550	4	...
HD 235858	4850	120	185	980	15.92	290	5	...
HD 213985	10300	27	380	near-ir excess
IRAS 23304+6147	5200	105	170	1440	16.03	240	7	...

to the star. From our finding of a relation between the observed molecular column density and the expansion velocity we know that this is not the case. Furthermore, we take the standard abundances to be the computed peak abundance for IRC +10216. No accurate prediction for molecular abundance of CH⁺ in AGB ejecta was found in the literature, while, in the interstellar medium the large observed abundance of CH⁺ is still not well understood (see Gredel et al. 1993 for a recent summary).

Using assumptions (i) and (ii) we will derive an equation for the mass-loss rate in a rather simple manner. Starting with the general formula for conservation of mass, $\dot{M}(r) = 4\pi r^2 \rho(r) v_{\text{exp}}(r)$, and assuming a constant mass-loss rate over time, $\rho(r) = \rho_0 (r_0/r)^2$, we find for the density at the dust inner radius::

$$\rho_0 = \frac{N_{\text{mol}}}{r_0} \cdot \frac{\mu m_p}{X_{\text{mol}}} \quad (8)$$

where μ is the average hydrogen (molecular, atomic, and ionic) particle mass in units of m_p and N_{mol} the molecular column density. For the densities and temperatures expected in the AGB ejecta most hydrogen will be in the form of H₂ ($\mu = 2.0$). In the model of Cherchneff et al. (1993) the molecular particle abundances relative to $n_H = n(\text{H}) + 2 \times n(\text{H}_2)$ are $X_{\text{C}_2} = 4 \times 10^{-6}$ and $X_{\text{CN}} = 3 \times 10^{-6}$. Combining Eqs. 5 & 8 yields the expression for the mass-loss rate:

$$\begin{aligned} \dot{M} = & \left(4\pi \mu m_p R_\odot T_\odot^2 \sqrt{\frac{L_*}{L_\odot}} \right) \cdot \frac{N_{\text{mol}}}{X_{\text{mol}}} \cdot \left(\frac{T_{\text{dust}}}{0.6} \right)^{-\left(\frac{4+p}{2}\right)} \cdot \\ & (T_{\text{eff}})^{\frac{p}{2}} \cdot v_{\text{exp}} = \\ & 3.71 \times 10^{-29} \cdot \frac{N_{\text{mol}}}{X_{\text{mol}}} \cdot T_{\text{dust}}^{-\frac{5}{2}} \cdot v_{\text{exp}} \cdot \sqrt{T_{\text{eff}}} \quad (9) \end{aligned}$$

with all parameters in cgs units except \dot{M} which is in M_⊙ yr⁻¹:

The mass-loss rates (assuming $\log L_* = 3.86 \log L_\odot$) derived in this manner (with the theoretical abundances of IRC 10216) are of the order of $-6.2 \leq \log \dot{M} \leq -4.1$ (Table 5), which is of the same order of magnitude as derived from the CO emission and the IR excess. In view of the important assumptions made in the calculation of the mass-loss rate we adopt an estimated error of one order of magnitude. We want to stress again that the assumption made in calculation the mass-loss rate from the molecular absorption lines only allow an order of magnitude estimate of the mass-loss rate. We want above all to show that these molecular lines do allow the determination of the mass-loss rate given the right inner and outer radius and the molecular abundance. If the mass-loss rate is known (from e.g., CO or infrared) the process can be reversed and this would yield the molecular abundance.

A linear least-squares fit (excluding IRAS 08005-2356, IRAS 05341+0852, and IRC +10216 for C₂ and CN and HD 235858 for CN) yields:

$$\log \dot{M}(\text{C}_2) = 0.11 \times v_{\text{exp}}(\text{C}_2) - 6.71 \quad (10)$$

$$\log \dot{M}(\text{CN}) = 0.13 \times v_{\text{exp}}(\text{CN}) - 5.86 \quad (11)$$

with correlation coefficients of 0.95 and 0.92, respectively. The mass-loss rate and velocity are in units of [M_⊙ yr⁻¹] and km s⁻¹ respectively.

4. Discussion

4.1. General discussion

We discuss the following points:

1. Within our sample of stars, eleven stars exhibit C₂ and CN absorption, one CH⁺ absorption, and one CH⁺

emission. All post-AGB stars with the Phillips bands in absorption also show the Swan bands in absorption. Since the $a^3\Pi_u$ state is 612 cm^{-1} above the ground state, corresponding to $J'' = 18$ in the $X^1\Sigma_g^+$ state, it is likely that this state is populated by optical pumping. A study of the Swan band will be subject of a separate paper.

2. We note that all the detected molecular bands are clearly detected, while the non-detections have no molecular bands or their strength is below our detection limit. It therefore seems that there is no star with intermediate strength molecular bands. Whether this is due to small number statistics or gives clues about circumstellar chemistry is to be evaluated in follow-up research. A suggestion for the latter option could be that the CSE is rather clumpy and that only clumps having a density higher than a critical value are able to sustain the presence of these molecules. On the other hand one might suggest that these molecular bands are rather common, but that our sample is too small to include stars with molecular bands of intermediate strength.

3. All stars exhibiting the unidentified $21\text{ }\mu\text{m}$ infrared features show the presence of C₂ and CN absorption, but this is not true for the reverse. The exception, IRAS 08005-2356, has the highest column density of C₂ in our sample, and exhibits OH maser emission at the same velocity. At the time of the observation, IRAS 05341+0852, was the only $21\text{ }\mu\text{m}$ sources not included in our sample. A recent study on the optical spectrum of this star by Reddy et al. (1997) has indeed show the presence of circumstellar C₂ and CN absorption.

We therefore predict that the recently found Post-AGB $21\text{ }\mu\text{m}$ sources (IRAS 22574+6609, Hrivnak & Kwok 1991a, IRAS 15553-5230 and IRAS 17195-2710, Henning et al. 1996, SAO 163075, Justtanont et al. 1996) will show C₂ and CN absorption. Whether the other new candidate and waiting list $21\text{ }\mu\text{m}$ stars (YSO and HII regions) listed by Henning et al. show molecular absorption, needs to be investigated. But if they do, then there is a one-to-one relation between the occurrence of the $21\text{ }\mu\text{m}$ emission feature and the presence of C₂ and CN absorption.

We did not found any clear correlation between the parameters listed in Table 5 and the strength of the $21\text{ }\mu\text{m}$ feature (Justtanont et al. 1996, Henning et al. 1996). Though there is a suggestion for an anti-correlation between the $N(\text{CN})/N(\text{C}_2)$ and $I(20\text{ }\mu\text{m})/I(18\text{ }\mu\text{m})$. Unfortunately, small number statistics do not allow any firm conclusion.

4. The presence of C₂ and CN or CH⁺ seems to be correlated with the dust color temperature: $T_{\text{dust}} \leq 300\text{ K}$ and $T_{\text{dust}} \geq 300\text{ K}$ respectively. C₂ and CN are correlated with cold dust (far-infrared excess) and CH⁺ with hot dust (near-infrared excess). This idea is supported by the rotational temperature of the heteronuclear species: $T_{\text{rot}} \approx 34$ and 200 K for CN and CH⁺ respectively.

5. The stars in our sample typically left the AGB 300 years ago and evolved to the left in the HR dia-

gram with a typical annual temperature increase of 5 K . IRAS 08005-2356 has an average annual temperature increase of 70 K per year. We predict that we can see evolutionary changes of the star and the CSE in the next 20 years.

6. Traditionally, the expansion velocities of the AGB ejecta are determined from the full width of the CO($J = 1 \rightarrow 0$) millimeter line profile. Since CO is abundant throughout the whole AGB ejecta, the profile contains the integrated emission. In the case of expansion velocities derived from line absorption, e.g., C₂, CN, and CH⁺, the line-forming region is along the line-of-sight towards the stellar photosphere. A second important difference is that the molecules observed in absorption are only present in a thin shell of material where the conditions are such that the molecule has a large abundance. This allows us to study the AGB ejecta at different radii, using different molecules. Unfortunately, from a theoretical study on the extended envelope of IRC+10216 (Cherchneff et al. 1993), it seems that the line-forming regions of C₂ and CN are almost the same. The upper panels of Fig. 4 clearly show the correlation between CO and the C₂ and CN expansion velocity, the relations are given in Eqs. 1 and 2. This unambiguously proves that the molecular absorption lines originate in the AGB ejecta and that these are thus circumstellar.

7. The lower panels of Fig. 4 show that the C₂ column density increases as a function of expansion velocity (Eqs. 3 and 4). To interpret this result, it is important to realize that the line-forming region of C₂ is only a thin shell. The inner radius is determined at a critical dust column density such that stellar and/or interstellar photons can penetrate and photodissociate complex molecules like C₂H₂ (via C₂H) and HCN into C₂ and CN, while the outer radius is determined in a similar way for the photodissociation of C₂ and CN to individual atoms by the interstellar and/or stellar radiation field. First, we will address the question of which radiation field (stellar, interstellar, or circumstellar) is responsible for the excitation and the photodissociation of C₂ and CN. Fig. 9 shows the interstellar radiation field (Draine (1978) for $\lambda \leq 2000\text{ }\text{\AA}$ and van Dishoeck & Black (1982) for $\lambda \geq 2000\text{ }\text{\AA}$), and a $T_{\text{eff}} = 6500\text{ K}$ stellar model (Kurucz 1979) with a $T_{\text{dust}} = 200\text{ K}$ dust shell. The radiation field of the star is scaled to a post-AGB star of $\log L = 3.86 \log L_{\odot}$ observed at a typical dust inner radius of $r_o = 2354\text{ R}_{\odot}$. For wavelengths $\lambda \geq 1400\text{ }\text{\AA}$ the stellar radiation field dominates, while for $\lambda \leq 1400\text{ }\text{\AA}$ the interstellar radiation field dominates. Since C₂ is pumped by optical radiation ($1300\text{ }\text{\AA}$ to $1.1\text{ }\mu\text{m}$), the stellar radiation field is responsible for the excitation of this molecule. Since the CN molecule can only be photodissociated by photons with $\lambda \leq 1100\text{ }\text{\AA}$, the interstellar ultraviolet radiation field photodissociates CN. The C₂ molecule is photodissociated by photons with $\lambda \leq 2000\text{ }\text{\AA}$ and can therefore be dissociated by both the ultraviolet interstellar and stellar radiation field.

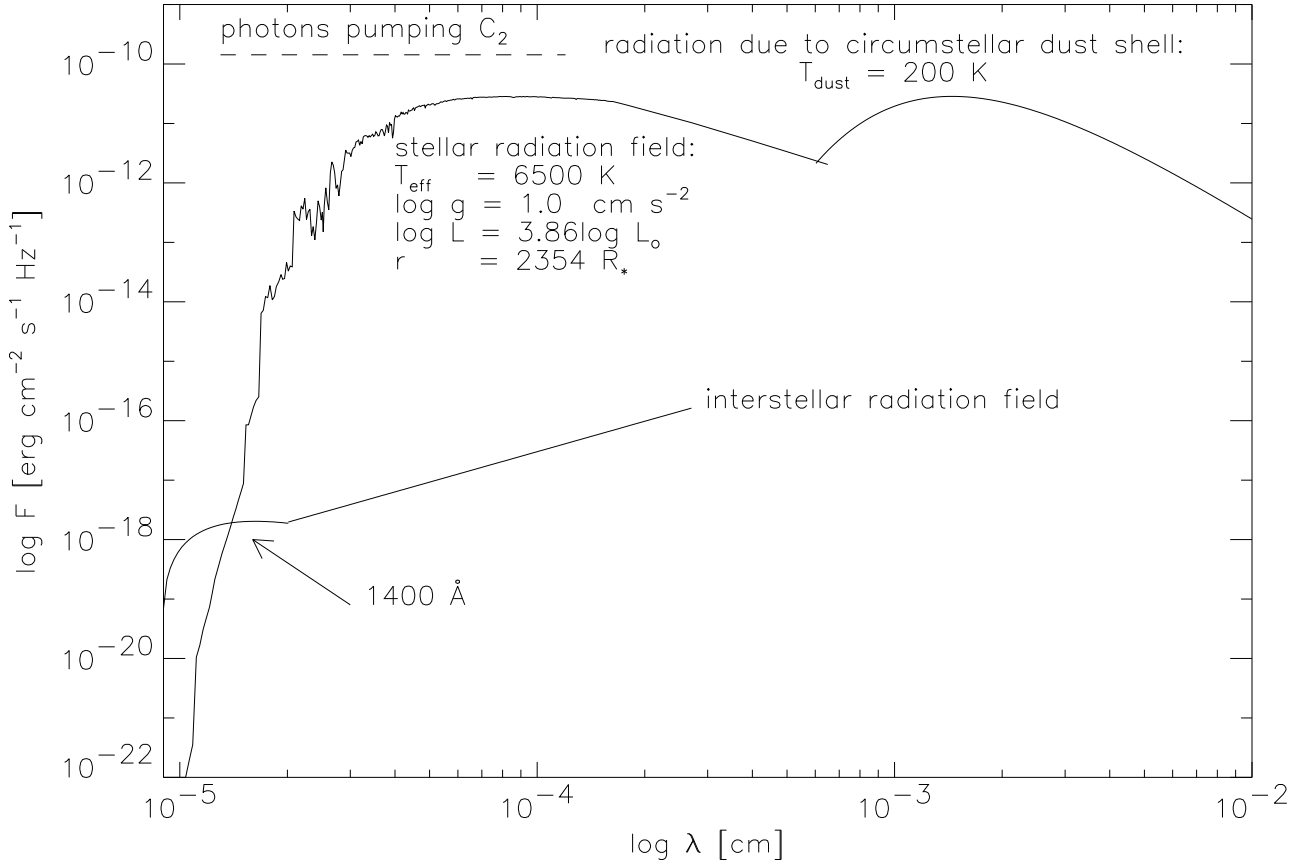


Fig. 9. The interstellar radiation field (solid straight line) and the stellar radiation field at $r_o = 2719 R_*$ of a $T_{\text{eff}} = 6500$ K, $\log g = 1$ Kurucz model. A typical infrared excess has been visualized by a $T_{\text{dust}} = 200$ K black-body (scaled arbitrarily). Optical pumping of C₂ uses photons between 1300 \AA and $1.1 \mu\text{m}$ (horizontal dashed line), while photodissociation of C₂ and CN needs photons with $\lambda \leq 2000$ and 1100 \AA , respectively.

We have clearly found a relation between the expansion velocity and the column density of C₂ and to a lesser extend of CN. The sign of the slope is inconsistent with models which assume a constant carbon abundance and mass-loss rate: these models predict a decrease in column density for increasing expansion velocities.

Alternatively we propose two models:

Our favorite model (model I): The radiation pressure efficiency (\overline{Q}_{rp} see Tielens 1983) scales with the carbon abundance. Since the momentum equation gives a positive correlation between \overline{Q}_{rp} and the acceleration dv_g/dr , this would account for the spread in the observed expansion velocities. At the same time the spread in carbon abundance in the ejecta will be observable as a spread in the observed column densities in a way consistent with our findings. We ran some simple models and found that only a small increase of \overline{Q}_{rp} gave rise to a significant change in expansion velocity. Additional and much more detailed modeling is needed to determine the exact relation be-

tween v_{exp} , $\log N$, and \overline{Q}_{rp} .

We propose an alternative model (model II): The higher the initial mass of the star, the higher the mass-loss rate and terminal velocity of the wind when the star terminates the AGB evolution (Barnbaum et al. 1991). Since an increase in mass-loss rate increases the column density, but an increase of the expansion velocity decreases it, the model can only explain the observation if the increase of mass-loss rate dominates over the increase of the expansion velocity. Since the number of thermal pulses increases with the mass of the progenitor, we also expect an increase of carbon abundance which would work in favor of this model. Therefore model II included the effect discussed for model I.

Since the model with the least free parameters is stronger than a more complex model, we favor model I and argue that a high C₂ (and CN) abundance reflects a high carbon abundance (and the C/O ratio), which in turn implies that the stars have experienced different amounts

(number or efficiency) of third dredge-ups. This hypothesis implies that there should be a relation between the carbon abundance of the star and the observed column density of circumstellar C₂.

We further note that there seems to be a flattening (possibly due to saturation of the absorption lines, flat part of curve of growth) in the molecular column densities for $v_{\text{exp}} \geq 30 \text{ km s}^{-1}$, but whether this is real or an artifact of small number statistics is not clear at this moment.

8. There should be a reasonable explanation why the relation between $\log N$ and v_{exp} for CN is not as well defined as for C₂. Although the CN molecular spectra are more complex than the C₂ spectra, and a unique identification of an absorption line with a single transition is not always possible, it is unlikely that this can account for the large scatter around the mean relation. Noting that all stars with $m_v \geq 12$ have $N(\text{CN})/N(\text{C}_2) \geq 3$, while all stars with $m_v \leq 12$ have $N(\text{CN})/N(\text{C}_2) \leq 3$, we suggest that the CN abundance might be affected by the distance of the star above the Galactic plane, and the local interstellar ultraviolet radiation field. It might also be that the fainter objects have a larger circumstellar reddening and therefore the molecules are more shielded against the stellar/interstellar radiation field. This would increase $N(\text{CN})$. However, information about the circumstellar reddening of these objects is not available.

9. Mass-loss rates have been derived from the observed column densities by making two very important assumptions. The basic conclusion is that the mass-loss rates determined are of the same order as those obtained from CO emission and infrared measurements, but do not allow a detailed comparison between different objects.

10. Federman et al. (1994) presented a relation between the C₂ and CN column density observed in diffuse interstellar clouds. We have investigated if this relation could be extrapolated to the conditions prevailing in the CSE of post-AGB stars (Fig. 10). We find (excluding IRC +10216, and IRAS 05341+0852):

$$\log N(\text{CN}) = 1.153 \times \log N(\text{C}_2) - 1.863 \quad (12)$$

with N in units of cm^{-2} with a low correlation coefficient of 0.43. Although both in the interstellar and circumstellar case C₂ and CN are primarily destroyed by photodissociation by the interstellar radiation field, the formation chemistry of these species is assumed to be very different in interstellar clouds.

11. We have searched for the lower v' bands (since they are the strongest); we did not detect a single isotopic line of C₂, CN, or CH⁺. Depending on the spectrum the detection limit is about 5 to 10 mÅ, which gives a typical lower limit of $^{12}\text{C}/^{13}\text{C} > 20$. ^{13}C is produced by the CN-cycle and not by the triple- α process. A high isotope ratio indicates that the carbon enhancement is due to the third-dredge up (convection reaches the deeper He-burning shell). This is rather surprising since one would

naively expect that the material from the outer shell (H-burning) can be dredged-up easily. The high isotope ratios of these stars is consistent with carbon stars (AGB stars) to be the progenitor of the stars studied ($^{12}\text{C}/^{13}\text{C} \approx 40 - 80$, Lambert et al. 1986). The third dredge-up only occurs on the thermal pulsating AGB phase for stars with $M_{\text{MS}} \leq 5 M_{\odot}$ ($Z = 0.001$): this sets an upper limit on the star's initial main sequence mass. For higher initial masses, Hot Bottom Burning (HBB) will prevent the formation of a carbon rich post-AGB star (Boothroyd et al. 1993).

12. Ultraviolet: Lambert et al. (1995) have obtained HST spectra of diffuse interstellar clouds, showing the Mulliken (0-0) (2313 Å) and F-X (0-0) (1342 Å) bands of C₂ in absorption. CO (e.g., 1509 and 1478 Å) and excited H₂ (e.g., 1108 and 1092 Å) are also prominent absorbers in the UV, since the column densities in the AGB ejecta are about two orders of magnitude larger than for interstellar clouds, the ultraviolet spectra of post-AGB stars as measured, e.g. with the HST and IUE, should be dominated by molecular (absorption) bands.

13. Visual: We predict the presence of the CN Violet system and the C₃ Swing system. Many molecules have been observed in the optical spectra of Comets. Though these are O-rich environments we would expect some of these molecules also to be present in C-rich environments. We therefore suggest the presence of the Merrill-Sandford SiC₂ bands (4640 and 4977 Å), CH (3130-3150 Å) and NH (3358 Å).

14. Infrared: Molecules have many transitions in the infrared. For the stars in our sample we might expect molecular absorption and emission in the infrared of e.g., H₂ (2-6 μm), HCN (3.4 μm), HCN (14.1 μm), C₂H (27.1 μm), C₂H₂ (13.6-13.8 μm).

13. Millimeter: Only for the strongest transitions of abundant molecules are lines in the optical and ultraviolet spectra observed. Many molecular transitions have been observed in the (sub-)millimeter and radio for IRC +10216 (for details see Kawaguchi et al. 1995), but very little work has been done to look at molecules in these wavelengths for post-AGB stars. However, to determine accurate abundances and to understand the circumstellar chemistry of detached dust shells, observations such as those presented here are of crucial importance.

4.2. Discussion of individual objects

IRAS 04296+3429: Very typical in its circumstellar CN and C₂ absorption.

IRAS 05113+1347: Very typical in its circumstellar CN and C₂ absorption. Our spectra show photospheric CN bands.

IRAS 05341+0852: This star has an overabundance of s-process elements and carbon (Reddy et al. 1997) which clearly suggests that this is a post-AGB star. Because of

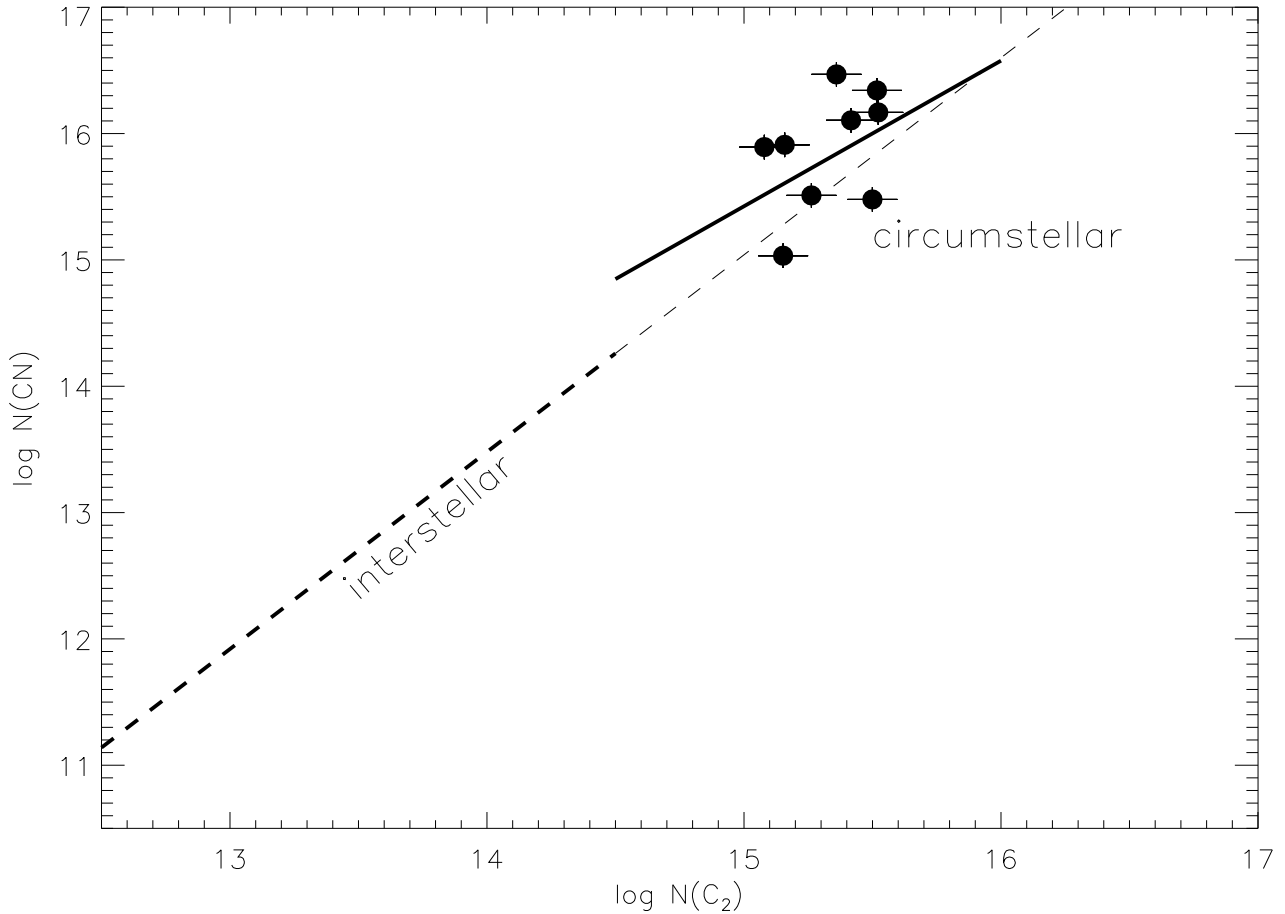


Fig. 10. A logarithmic plot of $N(\text{CN})$ versus $N(\text{C}_2)$. The thick dashed line represents the interstellar data points from Federman et al. (1994), while the circumstellar data points are determined in this study. It seems that the circumstellar points follow the interstellar trend.

the noisy spectra the data on C₂ and CN is not of the same quality as those for the other stars.

HD 44179 (The Red Rectangle): We confirm the presence of CH⁺ (0,0) and (1,0) in emission at a projected expansion velocity of $3.4 \pm 2.0 \text{ km s}^{-1}$ with $T_{\text{rot}} = 202 \pm 16 \text{ K}$, and the non-detection of C₂ and CN. CH⁺ in the Red Rectangle was first detected by Waelkens et al. (1992) and later identified by Balm & Jura (1992) and Hall et al. (1992) and is so far the only object which shows CH⁺ in emission. The latter authors estimated the rotational temperature to be $T_{\text{rot}} = 120 \pm 50 \text{ K}$. We prefer our determination of the rotational temperature since many more lines are included and the error on the equivalent width is significantly smaller.

Although we did not detect CN nor C₂, the latter molecule is observed in emission in the reflection lobes of the Red Rectangle (Sarre 1996). Schmidt et al. (1980) found numerous narrow features in the emission spectrum of the lobes, but were not able to make a proper identification. Glinsky et al. (1996a) review these unidentified

molecular bands and argue that they are due to phosphorescence of C₃. Glinsky et al. (1996b) report on their detection of the spin-forbidden Cameron bands of CO in the ultraviolet.

The absence of C₂ and CN absorption could be related to the low CO/I(60 μm) ratio (van der Veen et al. 1993). Since CO is underabundant and the star itself is extremely metal-depleted this might be the result of the same process: condensation of gas and molecules on circumstellar dust grains. Jura et al. (1995) detected weak CO millimeter radiation at $v_{*,\odot} = 18.9 \pm 2.0 \text{ km s}^{-1}$ (being the heliocentric stellar velocity derived from CO emission) with $v_{\text{exp}} \approx 6 \text{ km s}^{-1}$. This is close to the CH⁺ central velocity and suggests that CH⁺ emission is exactly on the system velocity. In the spectra discussed CH⁺ emission lines are not resolved. New observations (Bakker et al. 1996d) at $R \approx 120,000$ resolve the line profiles of the stronger lines with a $FWHM \approx 8.5 \text{ km s}^{-1}$ and $FWHM \approx 15 \text{ km s}^{-1}$ (full width at which the emission falls below the detection limit). Since the formation of CH⁺ is probably due to

shocks in a circumbinary disk (the emission comes from levels 42000 K above the ground level), the *FWFM* is an indication for the turbulent and Keplerian velocity of the line forming region. The interstellar CH⁺ abundance is not very well understood. Early models (e.g., Elitzur & Watson 1980) have suggested that CH⁺ might be formed efficiently in shocked regions. Although such models are currently not favored for the CH⁺ production in interstellar clouds, it could take place in the complex environment of the Red Rectangle. The fact that no absorption component is observed suggests that the line-forming region is not very extended and is within the “slit” of the telescope ($\leq 2''$).

It is interesting to note that the diffuse interstellar bands are in emission (Sarre 1991), although we did not find these bands in emission in our spectrum. Roddier et al. (1995) have spatially resolved the near-infrared emission into two separate emission peaks with an angular separation of $0.14''$. Waelkens et al. (1996) have clearly demonstrated that it is a single-lined spectroscopic binary with an orbital period of 318 ± 3 days. The latter authors argue that the star is not directly observed but only via scattered light on the reflection lobes.

HD 52961: Like the Red Rectangle and HD 213985, the photospheric abundance pattern shows evidence for selective accretion of circumstellar gas, but unlike these two other objects, no CH⁺ has been detected.

HD 56126: The C₂ and CN bands have been studied in detail in Paper I. It was shown that optical depth effects are important and that the excitation of C₂ is a balance between radiative and collisional (de-)excitation. HD 56126 has 21 (Kwok et al. 1989) and 30 μm features (Omont et al. 1995) and shows many of the s-process elements in its spectrum (Klochova 1995). Oudmaijer & Bakker (1994) suggested a pulsation period between 30 and 96 days. More recently Lèbre et al. (1996) discuss the possible RV Tauri nature of HD 56126, and they suggest the presence of four periods (32.9, 27.3, 11.9, and 7.1 days). We did a similar analysis with the data available from Lèbre et al. and some of our own data and confirm the presence of four significant minima in the Phase Dispersion diagram on the radial velocities of HD 56126. However, it seems possible that there is only one period of $P_{\text{puls}} = 12.1$ days and that the other minima are (sub-)harmonics.

IRAS 08005-2356: Slijkhuis et al. (1991) have shown that in the optical spectrum all absorption lines are blue-shifted up to velocities of 50 km s^{-1} . They interpreted this as a wind spectrum resulting from a huge post-AGB mass-loss rate of about $10^{-6} M_{\odot} \text{ yr}^{-1}$ with a terminal velocity of about 400 km s^{-1} . The H α profile shows significant changes within a time interval of less than two months which suggests a strong asymmetric mass-loss. The AGB ejecta emit OH maser emission with a maximum (projected) velocity of 50 km s^{-1} (Te Lintel Hekkert 1991), and the infrared energy distribution shows the presence of

a cold dust shell ($R \geq 3100 R_{*}$, $T_{\text{dust}} \leq 150 \text{ K}$) and a hot dust shell (or disk) at $R \geq 34 R_{*}$ with $T_{\text{dust}} \leq 1200 \text{ K}$. The overall observational characteristics of IRAS 08005-2356 are very similar to those of HD 101584 and suggest that the model by HD 101584 of Bakker et al. (1996b), consisting of a close binary system with an eccentric orbit also applies to IRAS 08005-2356. The secondary triggers the high-mass loss of the primary and the stellar wind acts as a curtain in front of a star much hotter than F5I. This suggests that the optical spectrum probably does not contain information about the star, but only about the wind.

The presence of C₂ and C₃ was also noted by Hrivnak (1995). Using our high-resolution spectra we are able to determine the expansion velocity of 50 km s^{-1} . C₂ absorption has the same radial velocity as the blue OH maser emission peak. The fact that the OH maser emission and C₂ are observed at the same velocity is unexpected since the first is a tracer of oxygen rich material (H₂O dissociation product), while the latter is an indicator of carbon-rich material (C₂H₂ dissociation product). This suggests that the star has only recently changed from oxygen to carbon-rich without changing its terminal wind velocity, or that there are separate carbon and oxygen rich mass-losing stars in the system, or that the circumstellar chemistry is very unusual. Bakker et al. (1996d) have observed the molecular absorption lines at a resolution of $R \approx 120,000$ and resolved the molecular features in two separate component with a line splitting of $5.7 \pm 2.0 \text{ km s}^{-1}$. The most likely explanation is that there are two photodissociation fronts at different velocities: one due to the stellar and one due to the interstellar radiation field. We further note that there are about twenty chromospheric narrow emission lines from neutral and singly ionized metals present in our spectrum, which are double peaked, consistent with an accretion disk. The presence of an accretion disk, and the accretion of material can generate a high velocity bipolar outflow.

We note that this is the only star in our sample which shows C₂ and CN but not the $21 \mu\text{m}$ feature. Very cautiously we propose that this object might have a $21 \mu\text{m}$ feature but that it was excluded from detection so far.

IRC +10216: Much of our knowledge about carbon-rich circumstellar environments is based on observing and modeling the carbon-rich AGB star IRC +10216. Over the years forty different molecular species have been identified in the radio and (sub)millimeter spectrum of this star (Lucas 1992). The mass-loss rate and expansion velocity have been determined from CO observations by Huggins et al. (1988) at $4 \pm 1 \times 10^{-5} M_{\odot} \text{ yr}^{-1}$ and $14 \pm 1 \text{ km s}^{-1}$. Circumstellar C₂ and visible lines of CN have not been reported and here we present the first detection of C₂ and possibly CN at an expansion velocity of $13.8 \pm 2.0 \text{ km s}^{-1}$ (Fig. 8). The spectrum is severely blended and an accurate determination of the continuum level and equivalent widths is impossible. Taking the local pseudo continuum as the continuum level we have determined equivalent widths and

derived $T_{\text{rot}} = 43 \pm 6$ K, $\log N = 14.90 \pm 0.10$ cm⁻², and $v_{\odot} = -33.3 \pm 0.7$ km s⁻¹, and $T_{\text{rot}} = 26 \pm 11$ K, $\log N = 14.90 \pm 0.10$ cm⁻², and $v_{\odot} = -32.3 \pm 0.7$ km s⁻¹ for the C₂ (2,0) and (3,0) bands, respectively. The theoretical work by Cherchneff et al. (1993) predicts $X_{\text{C}_2} = 4 \times 10^{-6}$ for a distance between 50 and 200×10^{15} cm. With a mass-loss rate of 3×10^{-5} M_⊙ yr⁻¹ and an expansion velocity of 14 km s⁻¹ (Huggins et al. 1988) this gives a column density of $\log N_{\text{predicted}} = 15.30$ cm⁻². Our observations are consistent with the predictions if we assume that the real continuum is a factor of three higher than the observed pseudo continuum. Alternatively, the C₂ abundance of Cherchneff et al. (1993) is a factor three too high.

HR 4049: This truly remarkable object is the most metal-depleted star known ([Fe/H] ~ -4.8, Waelkens et al. 1991). Bakker et al. (1996a) have studied the complete optical spectrum at high-resolution and high signal-to-noise ratio without detecting a single iron peak line. A strong near-infrared excess has been detected (Lamers et al. 1986) which is probably due to the presence of a circumbinary disk. However, unlike the Red Rectangle and HD 213985, no CH⁺ absorption or emission has been detected in HR 4049, which suggests that the post-AGB mass-loss, or mass-transfer in the binary system, is less violent and does not result in the presence of a shocked region of circumstellar gas.

HD 161796: An O-rich supergiant believed to be a post-AGB star. No molecules have been detected in the optical spectrum of this star.

IRAS 20000+3239: Not much is known about this object except that it exhibits the unidentified 21 μm (Kwok et al. 1995) and 30 μm (Omont et al. 1995) features. In the sample of stars with C₂ and CN absorption lines this is the star with the highest $N(\text{CN})/N(\text{C}_2)$ ratio of 11.2, the hottest CN rotational temperature of $T_{\text{rot}} = 50 \pm 12$ K, while it has a typical expansion velocity of 12.8 km s⁻¹. The CN column density relative to C₂ is about twice as high as the average. Our spectra show photospheric CN bands. We also note that the CO absorption in the K-band is the strongest in the sample of stars observed (Hrivnak et al. 1994).

AFGL 2688 (The Egg Nebula): This object is observed as a highly reddened central star surrounded by a torus (possibly a close binary system) with two bright lobes (reflection nebulae) at the equatorial poles of the system. Three different stellar winds are observed in the CO millimeter line emission (Young et al. 1992): high (HVW), medium (MVW) and low velocity wind (LVW) with expansion velocities of 100 ± 10 , 45 and 22.8 km s⁻¹, respectively. The HVW is bipolar with a de-projected wind velocity of 360 km s⁻¹. While the HVW and MVW are post-AGB winds, the LVW is the stellar wind when the star was on the AGB (now the AGB ejecta). From modeling of the CO millimeter emission Young et al. found that the AGB ejecta contain 0.7 M_⊙ fed by an AGB mass-loss rate of $\dot{M} = 1.5 \times 10^{-5}$ M_⊙ yr⁻¹.

C₂ emission was first reported by Crampton et al. (1975) and later confirmed by Cohen & Kuhi (1977). From optical spectropolarimetry, Cohen & Kuhi have shown that C₂ is in absorption in the reflected, polarized, light of the lobes and has an unpolarized emission component, which is attributed to emission within the “slit”. Crampton et al. also report C₃ absorption.

We have observed the brightest lobe (north lobe) of the Cygnus Egg Nebula and found C₂ in absorption with an expansion velocity of 17.3 ± 2.0 km s⁻¹. This indicates that C₂ (and CN) is formed in the LVW. However, we did not observe any emission, which is probably due to the smaller “slit length” used, so that only reflected light from the lobe is observed and no emission from the surrounding gas. Although reported by Cohen & Kuhi (1977), our spectra do not show the presence of the SiC₂ Merrill-Sanford band (4977 Å) in absorption.

We did not detect the ¹³CN Red System (1,0) band which places a lower limit of $^{12}\text{C}/^{13}\text{C} \geq 19$. This is consistent with the isotope ratio of $^{12}\text{C}/^{13}\text{C} \approx 20$ found by Wannier & Sahai (1987) in the slow wind. The fast wind has an isotope ratio of $^{12}\text{C}/^{13}\text{C} \approx 5$ (Jaminet & Danchi 1992). Jaminet & Danchi found a self absorption feature in the CN millimeter lines at the same velocity we find the optical absorption lines. This opens the possibility to study the CN molecule by both its optical absorption lines and the millimeter emission lines.

IRAS 22223+4327: Together with HD 235858 these are the only two sources in our sample which show the CO first overtone in emission. This is attributed to collisional excitation of the CO molecule in the circumstellar environment. C₂ and C₃ detections are reported by Hrivnak (1995). We confirm the presence of C₂ absorption and add CN to the list. As a result of the large number of observed molecular lines of C₂ the rotational temperature and column density are among the highest in our sample.

HD 235858 (IRAS 22272+5435): This photometric variable has an impressively strong far-infrared excess due to a detached dust shell. Together with the presence of strong absorption lines from s-processed elements this is clearly a post-AGB star (Začs et al. 1995). C₂ and C₃ absorption in the optical spectrum were first noted by Hrivnak & Kwok (1991b), while here we add CN to the list of detections. Very strong photospheric CN Red System bands lines (Bakker et al. 1996d) and narrow line circumstellar CN Red System bands are observed simultaneously (e.g. 7895 to 7905 Å). Hrivnak et al. (1994) reported on the change from CO first overtone absorption to emission in less than two months. Since CO first overtone bands are formed in hot gas ($T_{\text{gas}} \sim 1000$ K) it is not expected that circumstellar C₂ or CN will follow the variations of CO. HD 235858 differs from the other objects showing C₂ and CN absorption in that the CN abundance is the lowest in our sample. Since we have argued that the large spread in observed column densities of CN is probably due to differences in the UV radiation field it seems likely

that HD 235858 is exposed to a stronger interstellar UV radiation field than average.

HD 213985: The overall energy distribution is very much like that of HR 4049. Differences occur in the ultraviolet because of different circumstellar extinction laws, and in the far-infrared due to the presence of cool AGB ejecta. The infrared energy distribution of HD 213985 can be modeled using two Blackbodies: one component at a distance of $22 R_*$ with $T_{\text{dust}} = 1250$ K, probably a circumbinary disk, and a second component at $220 R_*$ with $T_{\text{dust}} = 350$ K, the AGB ejecta (Waelkens et al. 1987). Here we confirm the detection of CH⁺ in absorption at an expansion velocity of 6.7 ± 2.0 km s⁻¹ (Waelkens et al. 1995). If CH⁺ is formed in the AGB ejecta at a distance of $220 R_*$ (with $R_* = 50 R_\odot$) then HD 213985 left the AGB only 43 years ago. This would mean that the effective temperature has increased from 3500 K to 8500 K in 43 years giving an average annual increase of 100 K. Since this is not observed, CH⁺ cannot be formed in the AGB ejecta but is probably formed much closer to the star: a shocked region in a slowly expanding circumbinary disk.

We note that in our spectra of HD 213985 there is evidence for line splitting very similar to those observed for W Virginis stars (e.g., ST Pup and V29, Gonzalez 1993). Most noticeable the TiII lines at 4549.61 and 4563.77 show not only a narrow absorption feature on the red wing, but also the FeII displayed in Fig. 3.

BD +39°4926: This star is almost a twin of the central star of the Red Rectangle, with the difference that no infrared excess has been detected for this object. Unlike the Red Rectangle and HD 213985, no CH⁺ absorption or emission has been detected. This combined with the absence of an infrared excess suggests that the post-AGB mass-loss, or mass-transfer in the binary system, is less violent and does not result in the presence of a shocked region of circumstellar gas.

IRAS 23304+6147: Very typical in its circumstellar CN and C₂ absorption.

5. Conclusions

We have explored a new technique to study the physical and chemical conditions of the AGB ejecta by looking at molecular absorption and emission lines in the optical spectra of post-AGB stars. We find that all stars exhibiting the unidentified $21 \mu\text{m}$ feature have C₂ and CN absorption. Stars which show C₂ and CN do not show CH⁺ absorption. The presence of C₂ and CN is correlated with the presence of cold dust ($T_{\text{dust}} \leq 300$ K), while CH⁺ is correlated with the presence of hot dust ($T_{\text{dust}} \geq 300$ K).

The expansion velocities determined from the molecular absorption lines are in very good agreement with the expansion velocities derived from CO millimeter line emission. This proves that the molecular absorption lines are formed in the AGB ejecta. The absolute heliocentric velocity of the AGB ejecta in the line-of-sight can be de-

termined very accurately thanks to the large number of molecular lines available in the optical. We find a typical error of ~ 0.3 km s⁻¹ in our observations.

From the observed equivalent widths (see App. A, only at CDS) of the absorption lines the rotational temperatures and column densities can be determined. We find that the rotational temperature of C₂ is significantly higher than that of CN. C₂ is super-thermally excited, whereas CN is sub-thermally excited. This is consistent with the fact that C₂ is a homonuclear molecule (with $I = 0$) and CN a heteronuclear molecule, while the primary excitation mechanism of C₂ is optical pumping by the stellar radiation field. A more detailed analysis of the excitation of these species can lead to better constraints on the physical parameters in the AGB ejecta and to an independent determination of the mass-loss rate. These points will be further investigated in a subsequent paper (Paper III in preparation).

Interestingly, we found that the molecular column densities increase with expansion velocity. This is interpreted as due to the fact that carbon-rich dust is accelerated to higher velocities by the stellar radiation field. The observed column densities are an indicator of the molecular abundance. Mass-loss rates are computed which are of the same order of magnitude as those found from the IR excess and from CO emission lines. In view of the important assumption made to be able to compute the mass-loss rate, we stress that these rates should be cited cautiously.

Acknowledgements. The authors want to thank Henny Lamers, Christoffel Waelkens, René Oudmaijer, Hans van Winckel, Guillermo Gonzalez, Xander Tielens, John Mathis, and David Lambert for the stimulating and constructive discussions on this work. The significant contributions to this work by Jurien Veenhuis are very much appreciated. EJB (in the Netherlands) was supported by grant no. 782-371-040 by ASTRON, which receives funds from the Netherlands Organization for the Advancement of Pure Research (NWO), and (in the USA) in part by the National Science Foundation (Grant No. AST-9315124). LBFMW acknowledges financial support from the Royal Dutch Academy of Arts and Sciences. EvD is grateful to NWO for support through a PIONIER grant. This research has made use of the Simbad database, operated at CDS, Strasbourg, France.

References

- Bakker, E.J., Waters, L.B.F.M., Lamers, H.J.G.L.M., Schoenmaker, T. 1995, Ap&SS 224, 335
- Bakker, E.J., van der Wolf, F.L.A., Lamers, H.J.G.L.M., Gulliver, A.F., Ferlet, R., Vidal-Madjar, A. 1996a, A&A 306, 924
- Bakker, E.J., Lamers, H.J.G.L.M., Waters, L.B.F.M., Waelkens, C., Trams, N.R., van Winckel, H. 1996b, A&A 307, 869
- Bakker, E.J., Waters, L.B.F.M., Lamers, H.J.G.L.M., Trams, N.R., van der Wolf, F.L.A. 1996c, A&A 310, 893 (Paper I)

- Bakker, E.J., Lambert, D.L., van Dishoeck, E.F. 1996d, in press, IAU Symposium 177 on “The Carbon Star Phenomenon”, ed. R. Wing.
- Ballik, E.A., Ramsay, D.A. 1963, ApJ 137, 84
- Balm, S.P., Jura, M. 1992, A&A 261, L25
- Barnbaum, C., Kastner, J.H., Zuckerman, B. 1991, AJ 102, 289
- Blöcker, T. 1995, A&A 299, 755
- Boothroyd, A.I., Sackmann, I.J., Ahern, S.C. 1993, ApJ 416, 762
- Brocklehurst, B., Hébert, G.R., Innanen, S.H., Seel, R.M., Nicholls, R.W. 1971, “The identification atlas of molecular spectra: the CN A²Π – X²Σ⁺ Red System”, York University, Centre for Research in Experimental Space Science
- Carrington, A., Ramsay, D.A. 1982, Physica Scripta 25, 272
- Cherchneff, I., Glassgold, A.E., Mamon, G.A. 1993, ApJ 410, 188
- Cohen, M., Kuhi, L.V., 1977, ApJ 213, 79
- Draine, B.T. 1978, ApJS 36, 595
- Chauville, J., Maillard, J.P., Mantz, A.W. 1977, J.Mol.Spectr. 68, 399
- Crampton, D., Cowley, A.P., Humphreys, R.M. 1975, ApJ 198, L135
- Dyck, H.M., Benson, J.A., Howell, R.R., Joyce, R.R., Leinert, C. 1991, AJ 102, 200
- Elitzur, M., Watson, W.D. 1980, ApJ 236, 172
- Federman, S.R., Strom, C.J., Lambert, D.L., Cardelli, J.A., Smith, V.V., Joseph, C.L. 1994, ApJ 424, 777
- Fernie, J.D. 1995, AJ 110, 3010
- Glinski, R.J., Nuth III, J.A. 1996a, Ap&SS, submitted
- Glinsky, R.J., Nuth III, J.A., Reese, M.D., Sitko, M.L. 1996b, ApJ 467, 109
- Gonzalez, G. 1993, “A study of the UV-bright stars in Omega Cen and the type II Chepheid ST Pup”, Thesis University of Washington
- Gredel, R., van Dishoeck, E.F., Black, J.H. 1993, A&A 269, 477
- Hall, D.I., Miles, J.R., Sarre, P.J., Fossey, S.J. 1992, Nature 358, 629
- Henning, Th., Chan, S.J., Assendorp, R. 1996, A&A in press
- Herzberg, G. 1950, “Molecular Spectra and Molecular Structure, I. Spectra of Diatomic Molecules”, second edition
- Hrivnak, B.J. 1995, ApJ 438, 341
- Hrivnak, B.J., Kwok, S. 1991a, ApJ 368, 564
- Hrivnak, B.J., Kwok, S. 1991b, ApJ 371, 631
- Hrivnak, B.J., Kwok, S., Geballe, T.R. 1994, ApJ 420, 783
- Huggins, P.J., Olofsson, H., Johansson, L.E.B. 1988, ApJ 332, 1009
- IRAS catalogue, volume 1-6, Explanatory Supplement and Point Source Catalogue, Joint IRAS Science Work Group 1986, NASA RP-1190
- Jaminet, P.A., Danchi, W.C. 1992, ApJ 400, 535
- Jørgenson, U.G., Larsson, M. 1990, A&A 238, 424
- Jura, M., Balm, S.P., Kahane, C. 1995, ApJ. 453, 721
- Justtanont, K., Barlow, M.J., Skinner, C.J., Roche, P.F., Aitken, D.K., Smith, C.H. 1996, A&A 309, 612
- Kawaguchi, K., Kasai, Y., Ishikawa, S., Kaifu, N. 1995, PASJ 47, 853
- Klochova, V.G. 1995, MNRAS 272, 710
- Kodaira, K., Greenstein, J.L., Oke, J.B. 1970, ApJ 159, 485
- Kurucz, R.L. 1979, ApJS 40, 1
- Kwok, S., Volk, K., Hrivnak, B.J. 1989, ApJ 345, L5
- Kwok, S., Hrivnak, B.J., Geballe, T.R. 1995, ApJ 454, 394
- Lambert, D.L., Gustafsson, B., Eriksson, K., Hinkle, K.H. 1986, ApJ 62, 273
- Lambert, D.L., Sheffer, Y., Federman, S.R. 1995, ApJ 438, 740
- Lamers, H.J.G.L.M., Waters, L.B.F.M., Garmany, C.D., Perez, M.R., Waelkens, C. 1986, A&A 154, L20
- Langhoff, S.R. 1996, Private Communications
- Langhoff, S.R., Bauschlicher, Jr., Rendell, A.P., Komornicki, A. 1990, J.Chem.Phys 92, 3000
- Larsson, M., Siegbahn, P.E.M. 1983, Chem.Phys. 76, 175
- Lèbre, A., Maunon, N., Gillet, D., Barthès, D. 1996, A&A 310, 923
- Likkel, L., Omont, A., Morris, M., Forveille, T. 1987, A&A 173, L11
- Lucas, R. 1992, “Astrochemistry of Cosmic Phenomena”, ed. P.D. Singh (Dordrecht: Kluwer), page 389
- Marenin, I.R., Johnson, H.R. 1970, J.Quant. Spectrosc. Radiat. Transfer 10, 305
- Moore, Ch.E., Minnaert, M.G.J., Houtgast, J. 1966, The Solar Spectrum 2935 Å to 8770 Å, NBS Mono. 61
- Omont, A., Loup, C., Forveille, T., Te Lintel Hekkert, P., Habing, H.J., Sivagnanam, P. 1993, A&A 267, 515
- Omont, A., Moseley, S.H., Cox, P., Glaccum, W., Casey, S., Forveille, T., Chan, Kin-Wing, Szczerba, R., Loewenstein, R.F., Harvey, P.M., Kwok, S. 1995, ApJ 454, 819
- Oudmaijer, R.D., Bakker, E.J. 1994, MNRAS 271, 615
- Reddy, B.E., Parthasarathy, M., Gonzalez, G., Bakker, E.J. 1997, ApJ, accepted
- Roddier, F., Roddier, C., Graves, J.E., Northcott, M.J. 1995, ApJ 443, 249
- Sarre, P.J. 1991, Nature 351, 356
- Sarre, P.J. 1996, Private Communications
- Schmidt, G.D., Cohen, M., Margon, B. 1980, ApJ 239, L133
- Slijkhuis, S., Hu, J.Y., De Jong, T. 1991, A&A 248, 547
- Sopka, R.J., Hildebrand, R., Jaffe, D.T., Gatley, I., Roellig, T., Werner, M., Jura, M., Zuckerman, B. 1985, ApJ 294, 242
- Te Lintel Hekkert, P., Caswell, J.L., Habing, H.J., Haynes, R.F., Norris, R.P. 1991, A&AS 90, 327
- Tielens, A.G.G.M. 1983, ApJ 271, 702
- Trams, N.R. 1991, “Optically bright post-AGB stars”, Thesis University of Utrecht
- Tull, R.G., MacQueen, P.J., Sneden, C., Lambert, D.L. 1995, PASP 107, 251
- van der Veen, W.E.C.J., Trams, N.R., Waters, L.B.F.M. 1993, A&A 269, 231
- van Dishoeck, E.F., Black J.H. 1982, ApJ 258, 533
- van Winckel, H. Waelkens, C., Waters, L.B.F.M. 1995, A&A 293, L25
- Waelkens, C., Waters, L.B.F.M., Cassatella, A., Le Berte, T., Lamers, H.J.G.L.M. 1987, A&A 181, L15
- Waelkens, C., van Winckel, H., Bogaert, E., Trams, N.R. 1991, A&A 251, 495
- Waelkens, C., van Winckel, H., Trams, N.R., Waters, L.B.F.M. 1992, A&A 256, L15
- Waelkens, C., Waters, L.B.F.M., van Winckel, H., Daens, K. 1995, Ap&SS 244, 357
- Waelkens, C., van Winckel, H., Waters, L.B.F.M., Bakker, E.J. 1996, A&AL accepted
- Wannier, P.G., Sahai, R. 1987, ApJ 319, 367
- Woodsworth, A.W., Kwok, S., Chan, S.J. 1990, A&A 228, 503

- Young, K., Serabyn, G., Phillips, T.G., Knapp, G.R., Güsten, R., Schultz, A. 1992, ApJ 385, 265
- Začs, L., Klochkova, V.G. and Panchuk, V.E. 1995, MNRAS, 275, 764
- Zuckerman, B., Dyck, H.M., Claussen, M.J. 1986, ApJ 304, 401

A. Appendix: Equivalent width of C₂, CN, and CH⁺ lines

MS 5213

Circumstellar C₂, CN, and CH⁺ in the optical spectra of post-AGB stars

Eric J. Bakker, Ewine F. van Dishoeck, L.B.F.M. Waters, and Ton Schoenmaker

A&A main journal, 1997, volume, first page

molecular processes — circumstellar matter — stars: AGB and post-AGB — line: identification

Tables A.1/2/3/4/5 are available in electronic form at the CDS via anonymous ftp to cdsarc.u-strasbg.fr (130.79.128.5) or via <http://cdsweb.u-strasbg.fr/Abstract.html>, or from the authors

Description of parameters:

B	branch identification
J''	the rotational quantum number, total angular momentum including spin (Herzberg 1950)
N''	the rotational quantum number, total angular momentum excluding spin (Herzberg 1950) for CN: $J'' = N'' - 1/2$ (F ₂), $J'' = N'' + 1/2$ (F ₁)
λ	Laboratory wavelength of transition in air in Å=1e-10m
$f(J'J'')$	oscillator strength
EW	equivalent width in mÅ=1e-13m, positive values are absorption lines and negative values (only for HD 44179) are emission lines.

Branch identification for C₂ A¹Π_u – X¹Σ_g⁺ and CH⁺ A¹Π_u – X¹Σ_g⁺:

$B =$	–1	P Branch ($\Delta J = -1 = J' - J''$)
$B =$	0	Q Branch ($\Delta J = 0 = J' - J''$)
$B =$	1	R Branch ($\Delta J = 1 = J' - J''$)

Branch identification for CN A²Π – X²Σ⁺ (after Jørgenson & Larsson 1990):

$B =$	1	R ₁
$B =$	2	Q ₁
$B =$	3	P ₁
$B =$	4	^Q R ₁₂
$B =$	5	^P Q ₁₂
$B =$	6	^O P ₁₂
$B =$	7	R ₂
$B =$	8	Q ₂
$B =$	9	P ₂
$B =$	10	^S R ₂₁
$B =$	11	^R Q ₂₁
$B =$	12	^Q P ₂₁

Code used to identify a star:

*042	IRAS 04296+3429
*051	IRAS 05113+1347
*053	IRAS 05341+0852
*441	HD 44179
*561	HD 56126
*080	IRAS 08005-2356
*102	IRC +10216
*200	IRAS 20000+3239
*268	AFGL 2688
*222	IRAS 22223+4327
*235	HD 235858
*233	IRAS 23304+6147
*213	HD 213985

Tables:

Table A.1.	C ₂ A ¹ Π _u – X ¹ Σ _g ⁺ Phillips (2,0) band.
Table A.2.	C ₂ A ¹ Π _u – X ¹ Σ _g ⁺ Phillips (3,0) band.
Table A.3.a	CN A ² Π – X ² Σ ⁺ Red System (2,0) band.
Table A.3.b	Continued: CN A ² Π – X ² Σ ⁺ Red System (2,0) band.
Table A.4.a	CN A ² Π – X ² Σ ⁺ Red System (3,0) band.
Table A.4.b	CN A ² Π – X ² Σ ⁺ Red System (3,0) band.
Table A.5.	Continued: CH ⁺ A ¹ Π – X ¹ Σ ⁺ (0,0) band.

Table A.1. C₂ A¹Π_u – X¹Σ_g⁺ Phillips (2,0) band.

<i>B</i>	<i>J</i> ^{''}	<i>λ</i> (air) [Å]	<i>f</i> (<i>J</i> ^{''} <i>J</i> ^{''})	<i>EW</i> [mÅ] *102
1	6	8750.850	4.43E-04	44.3
1	8	8751.490	4.24E-04	
1	4	8751.687	4.80E-04	117.5
1	10	8753.581	4.11E-04	
1	2	8753.949	5.76E-04	77.1
1	12	8757.130	4.04E-04	
1	0	8757.686	1.44E-03	117.5
0	2	8761.197	7.20E-04	125.0
1	14	8762.147	3.98E-04	
0	4	8763.754	7.20E-04	118.2
-1	2	8766.031	1.44E-04	53.9
0	6	8767.762	7.19E-04	32.7
1	16	8768.631	3.92E-04	
0	8	8773.223	7.19E-04	
-1	4	8773.430	2.40E-04	29.6
1	18	8776.611	3.88E-04	
0	10	8780.144	7.18E-04	
-1	6	8782.311	2.76E-04	
1	20	8786.050	3.85E-04	
0	12	8788.561	7.17E-04	
-1	8	8792.652	2.96E-04	
1	22	8796.979	3.82E-04	
0	14	8798.462	7.17E-04	
-1	10	8804.502	3.07E-04	
1	24	8809.410	3.80E-04	
0	16	8809.844	7.16E-04	
-1	12	8817.830	3.15E-04	
0	18	8822.728	7.15E-04	
1	26	8823.379	3.78E-04	
-1	14	8832.682	3.20E-04	
0	20	8837.122	7.14E-04	
1	28	8838.846	3.76E-04	
-1	16	8849.075	3.24E-04	
0	22	8853.044	7.12E-04	
1	30	8855.876	3.73E-04	
-1	18	8866.997	3.27E-04	
0	24	8870.519	7.11E-04	
1	32	8874.466	3.72E-04	
-1	20	8886.487	3.29E-04	
0	26	8889.535	7.10E-04	
1	34	8894.623	3.70E-04	
-1	22	8907.545	3.30E-04	
0	28	8910.135	7.08E-04	
1	36	8916.400	3.68E-04	
-1	24	8930.172	3.31E-04	
0	30	8932.333	7.06E-04	
-1	26	8954.440	3.32E-04	
0	32	8956.139	7.04E-04	
-1	28	8980.336	3.33E-04	
0	34	8981.586	7.02E-04	
-1	30	9007.897	3.33E-04	
0	36	9008.705	7.00E-04	
-1	32	9037.150	3.33E-04	
-1	34	9068.086	3.33E-04	
-1	36	9100.823	3.32E-04	

Table A.3.a CN A²Π – X²Σ⁺ Red System (2,0) band.

<i>B</i>	<i>J</i> ^{''}	<i>N</i> ^{''}	<i>λ</i> (air) [Å]	<i>f</i> (<i>J</i> [′] <i>J</i> ^{''})	<i>EW</i> [mÅ]		
					*080	*102	*235
6	8.5	9	7952.261	4.49E-05			
6	7.5	8	7946.181	4.65E-05			
6	6.5	7	7940.433	4.71E-05			
6	5.5	6	7935.020	4.69E-05			
3	9.5	9	7934.855	1.36E-04			
5	8.5	9	7934.812	1.22E-04			
3	8.5	8	7930.849	1.27E-04			
5	7.5	8	7930.811	1.30E-04			
6	4.5	5	7929.943	4.46E-05			
3	7.5	7	7927.167	1.18E-04			
5	6.5	7	7927.134	1.40E-04			
6	3.5	4	7925.204	3.84E-05			
3	6.5	6	7923.813	1.08E-04			
5	5.5	6	7923.784	1.51E-04			
6	2.5	3	7920.804	2.56E-05			
3	5.5	5	7920.786	9.53E-05			
5	4.5	5	7920.762	1.61E-04			
3	4.5	4	7918.091	8.04E-05			
5	3.5	4	7918.071	1.70E-04	17.3		
3	3.5	3	7915.729	6.22E-05			
5	2.5	3	7915.714	1.75E-04	43.9		
2	9.5	9	7915.407	3.49E-04			
4	8.5	9	7915.364	7.82E-05			
3	2.5	2	7913.704	3.64E-05			
5	1.5	2	7913.692	1.64E-04			
2	8.5	8	7913.473	3.40E-04			
4	7.5	8	7913.435	8.68E-05			
9	8.5	9	7913.336	1.49E-04			
2	7.5	7	7911.856	3.29E-04			
4	6.5	7	7911.822	9.73E-05			
2	6.5	6	7910.559	3.18E-04			
4	5.5	6	7910.529	1.10E-04			
2	5.5	5	7909.584	3.05E-04			
4	4.5	5	7909.559	1.26E-04			
2	1.5	1	7908.966	2.08E-04			
4	0.5	1	7908.959	4.37E-04	65.1	39.4	
2	4.5	4	7908.934	2.91E-04			
4	3.5	4	7908.914	1.48E-04			
2	2.5	2	7908.622	2.50E-04	109.1	52.2	
2	3.5	3	7908.613	2.73E-04			
4	1.5	2	7908.611	2.45E-04			
4	2.5	3	7908.597	1.81E-04			
9	7.5	8	7908.172	1.43E-04			
1	0.5	0	7906.598	4.93E-04	36.1	37.9	36.9
1	1.5	1	7903.892	3.12E-04	47.2	71.5	18.2
9	6.5	7	7903.237	1.37E-04			
1	2.5	2	7901.520	2.59E-04	30.9		23.1
1	3.5	3	7899.481	2.37E-04	33.5		
9	5.5	6	7898.529	1.29E-04			
1	4.5	4	7897.771	2.26E-04	38.5		
1	5.5	5	7896.386	2.21E-04	15.7		
1	6.5	6	7895.326	2.18E-04			

Table A.3.b Continued: CN A²Π – X²Σ⁺ Red System (2,0) band.

<i>B</i>	<i>J''</i>	<i>N''</i>	λ (air) [Å]	$f(J'J'')$	<i>EW</i> [mÅ]		
					*080	*102	*235
12	9.5	9	7895.174	6.22E-05			
8	8.5	9	7895.131	3.42E-04			
1	7.5	7	7894.583	2.17E-04			
1	8.5	8	7894.158	2.17E-04			
1	9.5	9	7894.045	2.17E-04			
9	4.5	5	7894.043	1.21E-04			
12	8.5	8	7892.153	6.68E-05			
8	7.5	8	7892.116	3.32E-04			
9	3.5	4	7889.776	1.11E-04			
12	7.5	7	7889.360	7.14E-05			
8	6.5	7	7889.327	3.22E-04			
12	6.5	6	7886.792	7.60E-05			
8	5.5	6	7886.763	3.11E-04			
9	2.5	3	7885.725	9.84E-05			
12	5.5	5	7884.445	8.06E-05			
8	4.5	5	7884.420	2.99E-04			
12	4.5	4	7882.315	8.46E-05			
8	3.5	4	7882.295	2.88E-04	23.5	18.7	
9	1.5	2	7881.889	7.79E-05			
12	3.5	3	7880.400	8.78E-05			
8	2.5	3	7880.384	2.77E-04	38.2		
12	2.5	2	7878.697	8.76E-05			
8	1.5	2	7878.686	2.70E-04	54.1		
12	1.5	1	7877.205	7.79E-05			
8	0.5	1	7877.198	3.09E-04	28.8		
11	9.5	9	7874.878	1.14E-04			
11	0.5	0	7874.852	3.09E-04	37.1		
7	8.5	9	7874.835	1.93E-04			
11	1.5	1	7873.992	2.26E-04	51.1		
11	8.5	8	7873.987	1.23E-04			
7	0.5	1	7873.985	1.84E-04			
7	7.5	8	7873.949	1.90E-04			
11	2.5	2	7873.343	2.01E-04	41.3		
7	1.5	2	7873.332	1.73E-04			
11	7.5	7	7873.325	1.34E-04			
7	6.5	7	7873.292	1.86E-04			
11	3.5	3	7872.905	1.84E-04			
7	2.5	3	7872.889	1.73E-04			
11	6.5	6	7872.889	1.45E-04			
7	5.5	6	7872.860	1.82E-04			
11	4.5	4	7872.682	1.70E-04			
11	5.5	5	7872.676	1.57E-04			
7	3.5	4	7872.662	1.75E-04			
7	4.5	5	7872.652	1.78E-04			
10	0.5	0	7871.654	1.28E-04			
10	1.5	1	7868.667	1.07E-04	20.7		
10	2.5	2	7865.892	9.53E-05	21.2		
10	3.5	3	7863.333	8.60E-05			

Table A.4.a CN A²Π – X²Σ⁺ Red System (3,0) band.

<i>B</i>	<i>J</i> ^{''}	<i>N</i> ^{''}	λ (air) [Å]	<i>f</i> (<i>J'J''</i>)	<i>EW</i> [mÅ]							
					*042	*051	*053	*561	*200	*268	*222	*233
6	8.5	9	6987.583	1.98E-05								
6	7.5	8	6982.767	2.04E-05								
6	6.5	7	6978.223	2.08E-05								
3	9.5	9	6974.278	5.93E-05								
5	8.5	9	6974.244	5.33E-05								
6	5.5	6	6973.953	2.05E-05								
3	8.5	8	6971.045	5.57E-05								
5	7.5	8	6971.016	5.74E-05								
6	4.5	5	6969.958	1.96E-05								
3	7.5	7	6968.079	5.18E-05								
5	6.5	7	6968.053	6.18E-05								
6	3.5	4	6966.241	1.68E-05								6.5
3	6.5	6	6965.383	4.71E-05								
5	5.5	6	6965.360	6.62E-05								
3	5.5	5	6962.956	4.18E-05								
5	4.5	5	6962.937	7.08E-05					79.7			
6	2.5	3	6962.801	1.12E-05	11.5							
3	4.5	4	6960.801	3.53E-05								
5	3.5	4	6960.785	7.47E-05	8.2				70.3		73.2	53.2
2	9.5	9	6959.402	1.53E-04								
4	8.5	9	6959.369	3.45E-05								
3	3.5	3	6958.920	2.70E-05								
5	2.5	3	6958.908	7.68E-05	11.5	25.6	46.8	12.8	76.6	19.2	72.9	43.2
2	8.5	8	6957.753	1.48E-04								
4	7.5	8	6957.724	3.83E-05								
9	8.5	9	6957.622	6.54E-05								
3	2.5	2	6957.314	1.60E-05								
5	1.5	2	6957.305	7.19E-05	19.3	42.2		7.9	58.6	30.7	67.4	
2	7.5	7	6956.367	1.44E-04								
4	6.5	7	6956.340	4.28E-05								
2	6.5	6	6955.243	1.39E-04								
4	5.5	6	6955.220	4.84E-05								
2	5.5	5	6954.385	1.33E-04								
4	4.5	5	6954.366	5.55E-05								
2	4.5	4	6953.795	1.27E-04								
4	3.5	4	6953.779	6.50E-05								
2	1.5	1	6953.652	9.13E-05								
4	0.5	1	6953.646	1.92E-04		58.2						
9	7.5	8	6953.498	6.27E-05								
2	3.5	3	6953.475	1.20E-04								
4	2.5	3	6953.462	7.99E-05								
2	2.5	2	6953.427	1.10E-04								
4	1.5	2	6953.418	1.08E-04								
1	0.5	0	6951.821	2.15E-04	70.9	106.8		34.1	122.9	104.2	145.2	110.8
1	1.5	1	6949.770	1.36E-04	15.2		34.1	24.0	101.0	114.4	128.9	55.7
9	6.5	7	6949.568	5.98E-05								
1	2.5	2	6947.992	1.14E-04	20.9		42.0	14.3	152.5	66.9	115.7	44.3
1	3.5	3	6946.486	1.04E-04					96.4		87.1	37.7
9	5.5	6	6945.831	5.66E-05								
1	4.5	4	6945.251	9.91E-05								
1	5.5	5	6944.285	9.66E-05			67.0					
12	9.5	9	6943.727	2.74E-05								

Table A.4.b Continued: CN A²Π – X²Σ⁺ Red System (3,0) band.

<i>B</i>	<i>J''</i>	<i>N''</i>	λ (air) [Å]	$f(J'J'')$	<i>EW</i> [mÅ]							
					*042	*051	*053	*561	*200	*268	*222	*233
8	8.5	9	6943.693	1.50E-04								
1	6.5	6	6943.584	9.53E-05								
1	7.5	7	6943.147	9.48E-05								
1	9.5	9	6943.052	9.49E-05								
1	8.5	8	6942.970	9.48E-05								
9	4.5	5	6942.282	5.30E-05								
12	8.5	8	6941.241	2.94E-05								
8	7.5	8	6941.211	1.45E-04								
12	7.5	7	6938.950	3.14E-05								
8	6.5	7	6938.923	1.41E-04								
9	3.5	4	6938.920	4.87E-05	9.7				68.3			52.3
12	6.5	6	6936.850	3.35E-05								
8	5.5	6	6936.827	1.36E-04								
9	2.5	3	6935.742	4.32E-05						34.6	37.9	35.0
12	5.5	5	6934.936	3.55E-05								
8	4.5	5	6934.917	1.31E-04					53.9			
12	4.5	4	6933.209	3.71E-05	8.6							
8	3.5	4	6933.194	1.26E-04		14.0			76.0		54.8	43.5
9	1.5	2	6932.748	3.42E-05							33.4	
12	3.5	3	6931.667	3.85E-05								
8	2.5	3	6931.655	1.21E-04	14.2				97.4		84.6	41.5
12	2.5	2	6930.305	3.84E-05								
8	1.5	2	6930.297	1.18E-04	43.5		11.1	12.9	93.7	87.8	119.8	56.7
12	1.5	1	6929.124	3.42E-05								
8	0.5	1	6929.119	1.36E-04		56.9		18.9	111.9	80.8	100.4	37.4
11	9.5	9	6928.188	5.02E-05								
7	8.5	9	6928.155	8.46E-05								
11	8.5	8	6927.333	5.44E-05								
7	7.5	8	6927.303	8.30E-05								
11	0.5	0	6927.302	1.36E-04	35.5			27.1	85.7	107.1	85.1	
11	7.5	7	6926.673	5.89E-05								
11	1.5	1	6926.665	9.90E-05	37.9				95.0	32.0		
7	0.5	1	6926.659	8.06E-05			92.9					
7	6.5	7	6926.646	8.14E-05								
11	2.5	2	6926.206	8.84E-05			11.3	17.2				
11	6.5	6	6926.205	6.37E-05								
7	1.5	2	6926.197	7.60E-05	42.0				144.5			
7	5.5	6	6926.182	7.97E-05								
11	3.5	3	6925.929	8.11E-05			81.4					
11	5.5	5	6925.926	6.90E-05								
7	2.5	3	6925.917	7.58E-05	38.8				158.9			72.2
7	4.5	5	6925.907	7.81E-05								
11	4.5	4	6925.835	7.46E-05								
7	3.5	4	6925.819	7.67E-05								
10	0.5	0	6924.855	5.61E-05	58.5		62.0		44.2	92.7	96.8	
10	1.5	1	6922.587	4.74E-05	26.3				65.4	81.5	71.1	63.0
10	2.5	2	6920.501	4.18E-05					49.0			
10	3.5	3	6918.598	3.77E-05					0			

Table A.5. CH⁺ A¹Π – X¹Σ⁺ (0,0) band.

<i>B</i>	<i>J</i> ^{''}	<i>λ</i> (air) [Å]	<i>f</i> (<i>J</i> ['] <i>J</i> ^{''})	<i>EW</i> [mÅ]	
				*441	*213
1	4	4225.276	1.81E-03	-9.0	4.0
1	3	4225.701	1.94E-03	-14.3	10.8
1	5	4225.807	1.73E-03		
1	2	4227.064	2.18E-03	-12.7	30.0
1	6	4227.318	1.67E-03		
1	1	4229.351	2.72E-03	-25.2	18.8
1	7	4229.837	1.63E-03		
1	0	4232.552	5.45E-03	-18.0	37.6
1	8	4233.398	1.60E-03		
1	9	4236.417	1.58E-03		
0	1	4237.563	2.73E-03	-33.4	21.2
0	2	4239.381	2.73E-03	-28.1	18.7
0	3	4242.116	2.73E-03	-21.0	29.6
1	10	4243.787	1.56E-03		
0	4	4245.779	2.73E-03	-12.9	9.5
-1	2	4247.573	5.47E-04	-8.9	
0	5	4250.387	2.74E-03	-6.0	
1	11	4250.709	1.55E-03		
-1	3	4254.389	7.83E-04	-12.8	
0	6	4255.959	2.74E-03	-5.0	
1	12	4258.853	1.54E-03		
-1	4	4262.121	9.15E-04	-9.4	
0	7	4262.519	2.74E-03		
1	13	4268.281	1.53E-03		
0	8	4270.096	2.75E-03		
-1	5	4270.780	1.00E-03	-10.3	
0	9	4278.724	2.75E-03		
1	14	4279.063	1.52E-03		
-1	6	4280.385	1.06E-03		
0	10	4288.440	2.76E-03		
-1	7	4290.948	1.11E-03		
0	11	4299.286	2.77E-03		
-1	8	4302.502	1.14E-03		
-1	9	4315.078	1.17E-03		

$f(J', J'') = f_{abs}$ is the absorption oscillator strength
for emission $g_{J'} f_{em} = g_{J''} f_{abs}$